Jonathan C. Kern, BSc

Example of a Determination of the *in situ* Block Size Distribution based on Borehole Loggings and Surface Mappings

MASTER'S THESIS

For the award of the academic degree

Diplom-Ingenieur

Master programme Geotechnics and Hydraulics

submitted to the

Graz University of Technology

Advisors:

O.Univ.-Prof. Dipl.-Ing. Dr.mont. Wulf Schubert

Institute of Rock Mechanics and Tunnelling

Graz University of Technology

Dipl.-Ing. Alexander Kluckner

Institute of Rock Mechanics and Tunnelling

Graz University of Technology

Andreas Anjan Buyer, B.Sc. M.Sc.

Institute of Rock Mechanics and Tunnelling

Graz University of Technology

Graz, August 2017

Affidavit

I declare that I have authored this thesis independently, that I have not used other than the declared sources/resources, and that I have explicitly marked all material which has been quoted either literally or by content from the used sources. The text document uploaded to TUGRAZonline is identical to the present master‘s thesis.

Date

Signature

Acknowledgements

First of all, I would like to thank Professor Wulf Schubert, who has awakened my interest in rock mechanics and tunneling, made me deepen my interest in this fascinating field of engineering and gave me the opportunity to compose this thesis at his institute.

Furthermore, my thanks go to my advisers Alexander Kluckner and Andreas Buyer, who have provided an extremely good supervision during this work, have shown a lot of perseverance and patience and always gave me a smart input and had an open ear for me.

Particular thanks are due to ASFiNAG and Forstinger & Stadlmann ZT GmbH, namely Dipl. Ing. Klaus Mittermayr and Mag. Thomas Stadlmann, who have provided most of the raw data for this thesis.

My greatest thanks goes to my family and friends, who have supported me throughout the whole period of my studies and were also there for me in tough times. I could not have accomplished this thesis without you.

Abstract

The mean block size as well as the block size distribution of jointed rock mass is an important parameter in the field of geotechnical engineering. In rock mass characterization, as example, the block size enters rock mass classification systems. The *in situ* block size distribution is used for the design of support measures against rockfall or to design the blast concept of mining and quarrying. To determine the block size distribution, three dimensional models are commonly used to simulate a specific area of the rock mass. Key parameters for such modeling systems are mainly the joint orientation, the spacing and the persistence. These data are practically gained by outcrop measurements or on the basis of core data in combination with geophysical measurements. By means of a practical example, this thesis investigates the question, what effect statistical simplifications of these key parameters have on the calculated block size distribution. For this purpose, a deterministic reference model, which is purely based on core data and borehole data, was created with the program 3DEC. This model is then compared to other, simplified, statistical 3DEC models. Furthermore, the accuracy of analytical solutions to calculate the mean block volume are tested.

A comparison with block volumes measured on the surface shows that an accurate block size distribution based solely on borehole data can only be achieved if there is knowledge about the persistence.

The results of the various models show that certain statistical simplifications, such as the statistical grouping of single joints to joint sets, represent a sufficiently precise approximation. Other simplifications, such as the artificial reduction of the number of joint sets, can be problematic. The analytical calculation methods can partly provide reliable results for the average block volume, appropriate for certain applications.

Kurzfassung

Sowohl die mittlere Blockgröße als auch die Blockgrößenverteilung von zerklüftetem Gebirge können für diverse geotechnische Problemstellungen eine entscheidende Kenngröße darstellen. Für die Gebirgscharakterisierung mit Hilfe von Klassifizierungssystemen wird beispielsweise die Blockgröße auf verschiedene Arten berücksichtigt. Die Blockgrößenverteilung hingegen, findet zum Beispiel Anwendung bei der Dimensionierung von Schutzbauwerken gegen Steinschlag oder auch bei der Sprengmitteldimensionierung im Lagerstättenwesen.

Die Bestimmung der Blockgrößenverteilung erfolgt vorwiegend mit dreidimensionalen Modellen, die einen bestimmten Bereich des Gebirges simulieren. Ausschlaggebende Eingangsgrößen für solche Modellierungen sind Gefügeparameter wie Trennflächenorientierung, Trennflächenabstand und Persistenz. Diese Informationen werden in der Praxis durch die Kartierung von Felsaufschlüssen, oder durch Bohrkernanalysen in Kombination mit geophysikalischen Messungen gewonnen.

In dieser Arbeit wird an Hand eines Beispiels untersucht, welche Auswirkungen statistische Vereinfachungen der Eingangsdaten auf die berechnete Blockgrößenverteilung haben. Hierfür wurde zunächst mit dem Programm 3DEC ein deterministisches Referenzmodell erstellt, das rein auf Bohrkern- und Bohrlochdaten basiert. Dieses Modell wurde dann mit anderen, vereinfachten, statistischen 3DEC-Modellen verglichen. Zudem wurde die Genauigkeit von analytischen Berechnungsverfahren zur Ermittlung des mittleren Blockvolumens geprüft.

Ein Vergleich mit Blockvolumina, die an der Oberfläche gemessen wurden, zeigt, dass eine adäquate Blockgrößenverteilung, rein auf Bohrlochdaten basierend, nur dann berechnet werden kann, wenn Kenntnisse bezüglich der Persistenz vorliegen.

Die Ergebnisse der verschiedenen Modelle zeigen, dass gewisse statistische Vereinfachungen, wie die Zusammenfassung von einzelnen Trennflächen zu Trennflächenscharen, eine genügend genaue Näherung darstellen. Andere Vereinfachungen, wie die künstliche Reduzierung der Scharanzahl, können jedoch problematisch werden. Auch die analytischen Verfahren können teilweise für gewisse Anwendungen herangezogen werden.

Contents

List of Figures

List of Tables

Abbreviations

RQD	.....	Rock Quality Designation
SRF	.....	Stress Reduction Factor
RMR	.....	Rock Mass Rating
RMi	.....	Rock Mass index
GSI	.....	Geological Strength Index
DFN	.....	Discrete Fraction Network
NNW	.....	North–northwest
SSE	.....	South–southeast
ENE	.....	East–northeast
GT	.....	Ground type
KB	.....	Core drilling
ATV	.....	Acoustic televiewer
OTV	.....	Optical televiewer
DD	.....	Dip direction
3DEC	.....	3-dimensional distinct element code
S	.....	Spacing
SD	.....	Standard deviation
Set	.....	Joint set
P	.....	Persistence
V	.....	Block volume

Symbols

l_{frac}	.....	length of core pieces larger than 100 mm
l_{tot}	.....	total core length [cm]
J_n	.....	Joint set number [-]
J_r	.....	Joint roughness number [-]
J_a	.....	Joint alteration number [-]
J_w	.....	Joint water reduction factor [-]
V_b	.....	Mean block volume [-]
S_i	.....	Spacing [m]
γ_i	.....	Intersection angle between two joint sets [°]
p_i	.....	Persistence factor [-]
T	.....	Transformation factor [-]

1 Introduction

When a rock mass is subjected to tectonic forces, its formerly massive structure may change to a less compact one, i.e. cracks and faults form and leave behind a rock mass that consists of smaller and larger blocks. The distribution of the volume of these different blocks is called *in situ* block size distribution and the borders or separations are generally called joints. Since these joints tell a story of how exactly the forces have acted on the rock in the past, they are of major interest in tectonics and related geological fields.

In geotechnics, the distribution and characteristics of joints are none the less important, because they have a significant influence on the rock mass behavior from an engineering perspective.

Whenever geotechnical or geological engineers have to deal with jointed rock mass, the *in situ* block size distribution of the rock mass is important for several tasks. The main disciplines which operate with these block statistics are, for example, rock mass characterization, rockfall hazard analysis, mining and quarrying.

For rock mass characterization, the block size can be used to calculate homogenized rock mass parameters like compressive strength, tensile strength or the deformation modulus (Hoek et al., 1995). For rockfall hazard analysis, block parameters like size or shape are important for the design of support measures (e.g. installation of rock bolts) and damage protection measures (e.g. construction of rockfall protection barriers). In mining and quarrying, the natural size of single blocks have for example significant impact on the design of the blast concept.

Important parameters, which determine the block size distribution of a rock mass section are the joint orientation, the joint spacing and the joint persistence (Kim et al., 2006).

1.1 State of the art

Over the past decades, several concepts to determine in situ block sizes, have been introduced. Here we want to present three different major groups of research for engineering and scientific issues. All three groups set a focus on the in situ block size, either embedded as a parameter for rock mass classification systems, or with a direct approach by means of analytic formulae or three dimensional modeling.

1.1.1 Block sizes considered in classification systems

For geotechnical design, different methods for rock mass classification systems had been developed. All these different systems are based on index evaluations of geological and physical quantities, and also consider the block size of the rock mass in one way or another. Utilizing these indexes, or more precisely, the combination of these indexes, one can roughly estimate the fragmentation of the rock mass.

Following the rock mass classification method of the so-called Q-System of Barton et al. (1974), one uses the Rock Quality Designation (RQD) index, which is the ratio of $l_{\text{frac}>100\text{mm}}$ – the sum of length of core pieces (e.g. in the core box of the drilling) larger than 100 mm – to the total core length l_{tot}, i.e.

$$\text{RQD} = \frac{l_{\text{frac}>100\text{mm}}}{l_{\text{tot}}} \cdot 100\%. \tag{1.1}$$

The RQD is then related to the index for the number of joint sets J_n. The main index Q is the approximate block size times a ratio that represents discontinuity properties times a factor to consider the effect of the water pressure and reads

$$Q = \frac{\text{RQD}}{J_n} \cdot \frac{J_r}{J_a} \cdot \frac{J_w}{\text{SRF}}. \tag{1.2}$$

One year earlier, Bieniawski (1973) introduced the Rock Mass Rating (RMR) system. This classification system considers an approximation of the mean block size as well, but this time as a combination of RQD with a factor for the joint spacing. Together with other determining parameters like rock strength, discontinuity properties, water conditions and joint orientation, one evaluates the rock mass quality with an index of $0 - 100$.

Another rock mass classification system, the RMi (Rock Mass index), was developed by

Palmström (1995). This system is a combination of the intact rock compressive strength (σ_c) and a jointing parameter (JP) for the rock mass.

$$\text{RMi} = \sigma_c \cdot Jp. \tag{1.3}$$

The jointing parameter includes in addition to the joint roughness, alteration and size, also the block volume.

Finally, Hoek et al. (1995) established the Geological Strength Index (GSI), with which one can directly assigns a number from 0 to 100 according to the "rock mass quality". The original GSI chart only contains a scale for the spacing with a verbal description of the block size in the first place, which was later extended by Cai et al. (2004) with an additional scale for the block volume (figure 1.1). Hence, the block volume V_b is directly implemented in the classification system as a parameter for characterization.

1.1.2 Block sizes via analytic formulae

Another group of methods to determine block volumes is through analytic calculations. Palmström (2005) introduced a formula for the mean block volume V_b of jointed rock masses, however only allowing for three distinct joint sets.

$$V_b = \frac{S_1 \cdot S_2 \cdot S_3}{\sin\gamma_1 \cdot \sin\gamma_2 \cdot \sin\gamma_3}. \tag{1.4}$$

In equation 1.4, S_i refers to the average joint spacing of sets i and γ_i to the intersection angle between the joint sets, respectively (figure 1.2).

Later, Cai et al. (2004) expanded Palmstöm's formula with the term p_i to consider the persistence of the joint sets (equation 1.5). It should be remarked, that these two formulae do not cover any distributions of block sizes, just single values.

$$V_b = \frac{S_1 \cdot S_2 \cdot S_3}{\sin\gamma_1 \cdot \sin\gamma_2 \cdot \sin\gamma_3 \cdot \sqrt[3]{p_1 \cdot p_2 \cdot p_3}}. \tag{1.5}$$

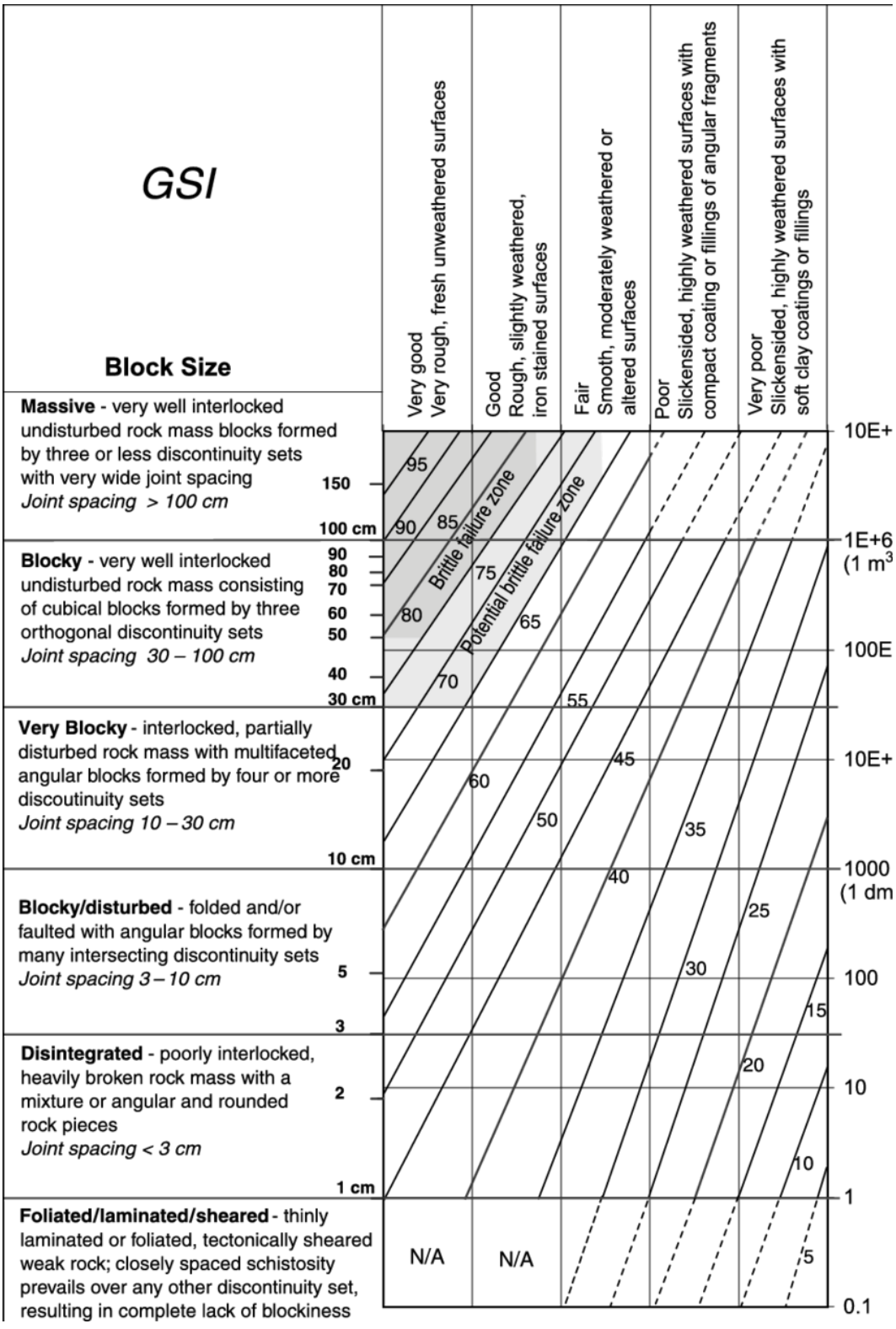

Figure 1.1: GSI chart with additional quantification for the block size (Cai et al., 2004).

To obtain more statistic values than the mean, Söllner (2014) introduced the transformation factor T, which depends on the average joint persistence:

$$V_{b(\text{mean},25\%,50\%,75\%)} = \frac{S_1 \cdot S_2 \cdot S_3}{\sin\gamma_1 \cdot \sin\gamma_2 \cdot \sin\gamma_3} \cdot T_{(\text{mean},25\%,50\%,75\%)}. \tag{1.6}$$

With this equation, one has the ability to calculate additional values for the 25 %-quantile, 75 %-quantile and the median (50 %-quantile).

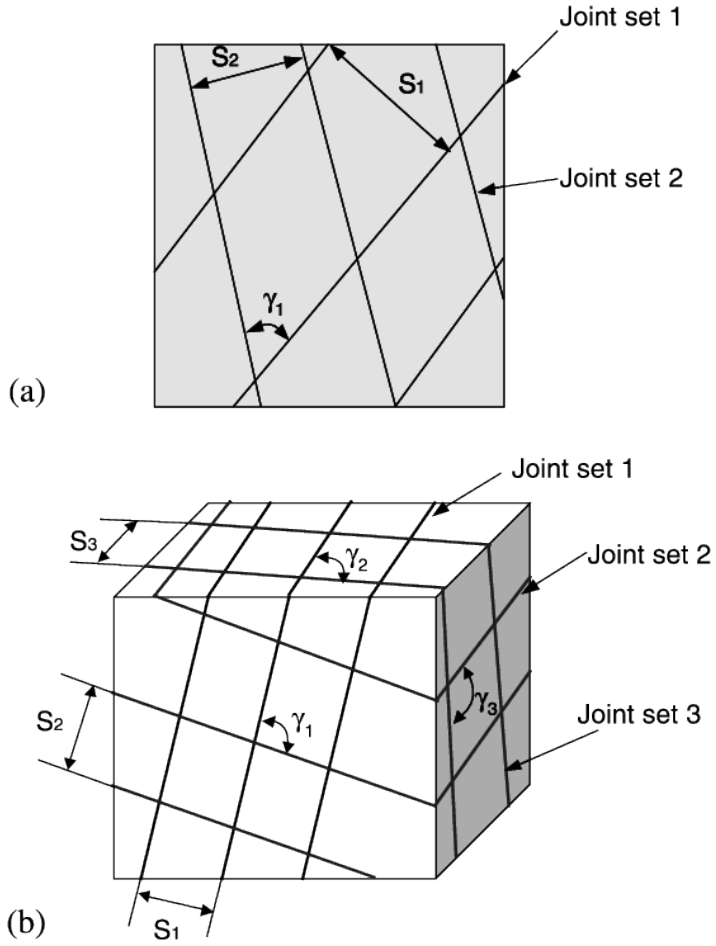

Figure 1.2: angles and spacing for analytic formula, 2-dimensional (a), 3-dimensional (b); (Kim et al., 2006).

1.1.3 Block sizes simulated with 3D models

The next level of research were 3D simulations of the block size distributions, either with analytic or numerical dissection models in combination with stochastic methods. The analytic approach of Wang et al. (2003), for example, can deal with any number of joint sets and with additional random joints. All blocks are individually sampled and some kind of persistence of the discontinuities is considered as well.

The most common numerical concepts are based on Discrete Fraction Network (DFN) modeling. DFN assumes all discontinuities as planar surfaces and the geometric input parameters like orientation, spacing, persistence or size as independent random variables, which are generated from certain probability distributions (Lei et al., 2017). Here, the location of the discontinuities is randomly determined. This method can be used for several approaches. Elmouttie & Poropat (2012) for example presented a polyhedral modeling algorithm for Monte Carlo simulation–based fracture models. The limitations of this statistical DFN method are, for instance, geometric oversimplifications and uncertainties in the statistic parameters (Lei et al., 2017).

As a part of this thesis, DFN was used for stochastic 3D modeling as well as for deterministic 3D modeling with discrete geometric input parameters.

1.2 Aim

This thesis aims to quantify different approaches to determine the *in situ* block size distribution of jointed rock mass. In order to create a realistic practical reference, data from an actual project were used, which is currently in progress. The provided data, which primarily contains basic geological information, field measurements, images of the drilling core samples and geophysical borehole analysis, is used to develop a 3D deterministic discontinuity model. This model, within certain limitations, shall be assumed as a realistic description of the *in situ* block size distribution and will be compared to results of simplified models and methods. Additionally, the block size distribution of the 3D underground models with surface measurements of block sizes are compared. Finally, an answer should be given whether and how these simplifications reflect on *in situ* block size distributions.

2 Project data

For the following investigations, we evaluated data of a current construction project in Austria. In this chapter we want to give a brief overview of the geological conditions of the area, the chosen subsurface area for specific studies and describe the types of provided geophysical data.
The geological information in the next section have been obtained from the non–public geological-, hydrological- and geotechnical report of the project, which can not be referenced due to confidentiality reasons.

2.1 Geology

The project area is located at the edge of the Bohemian Massif. The crystalline basement is overlaid with paleogene and neogene sediments, which are then again covered with quaternary sediments. This leads to the following simplified formation from top to bottom:

- recent deposits (scree)
- quaternary sediments
- neogene and paleogene sediments
- crystalline basement

Lithologically, the project area includes predominantly migmatites and paragneisses from the crystalline basement. As part of the Variscan orogeny, old paragneisses had been metamorphosed to “meta- to diatectic gneiss” and to “granitic diatexites”. Figure 2.1 shows a typical picture of the rock mass. Characteristic for this gneiss is a constant change between foliated zones and homogeneous granitic zones. The main mineralogical components are alkaline feldspar, plagioclase, quartz and mica.
The foliation of the gneiss is dominated mainly by layers of biotite. With the exception of

Figure 2.1: Outcrop of typical gneiss which can be found across the entire project area.

strongly foliated sections, the foliation itself has no major geomechanical relevance. In the project area, the foliation strikes generally NNW - SSE and dips mostly to ENE. Significant deviations from this direction can locally be caused by folding or flow structures. The intersection of the main joints with the foliation divide the rock mass into rhombic and prismatic rock blocks.

Referring to the guideline of the Austrian Society for Geomechanics (2010), three general ground types are distinguished, following the nomenclature shown in table 2.1. The key parameters for this classification are the degree of fracturing, degree of weathering, discontinuity properties and tectonic stress. A lithological distinction of the ground types by mineral composition, grain size or texture is not possible because of rock related variability and the frequent small-scale changes within the crystalline complex. However, such a distinction is not necessary due to similarity of physical properties.

2.2 Studied area

One of the main problems when measuring block size parameters is that one wants to create three-dimensional data from two-dimensional outcrops or one-dimensional geophysical measures from boreholes (Einstein & Baecher, 1983).

It is impossible to capture all joint orientations by the measurements. For this reason, an area was chosen where three boreholes exist in an uncommonly close range with different directions

Table 2.1: General classification of ground types in the project area.

Abbr.	Description	Rock Type	Remarks
GT 1	Crystalline rock – mostly fresh, low to moderately fractured.	Solid rock	Strong to very strong compressive strength; mostly favorable discontinuity properties (generally no infillings, undulate/stepped and rough surfaces).
GT 2	Crystalline rock – fresh to slightly weathered, moderately to very fractured.	Solid rock	Strong to very strong compressive strength; favorable to partly less favorable discontinuity properties (surfaces partly show fine-grained infillings) or locally weathered.
GT 3	Crystalline rock – partly moderately weathered or sheared, strong to very strong fractured.	Solid rock	Mostly medium strong to partly strong compressive strength, partly lowered by weathering or tectonic stresses; low to unfavorable discontinuity properties (surfaces show fine-grained infillings, partly smooth surfaces, weathered, open).

and inclinations to optimize the density of information (see table 2.2). For the present study, it was required to capture as many discontinuities as possible in the area. The maximum distance between the drilling start-locations is less than 7 m. For the numerical models, we chose different cubes with sides of 5 $m - 35$ m, so that the edges of the volumes are not far beyond the spatial drilling range. All cubes were located at a minimum of 10 m below the surface, such that their locations are underneath any soil– or loose–rock–zone. The dominant ground type of the investigated rock mass volume is GT2 (see table 2.1).

For to the field measurements, outcrops and rock blocks within the project area were considered as well, because the rock mass at the surface in general is homogeneous and a subdivision of the area into different sections is not necessary.

Table 2.2: Geometric parameter of the three investigated drillings.

Drilling	Depth [m]	Dip [°]	Dip Direction [°]
KB 1	86.4	90	0
KB 2	77.0	70	23
KB 3	95.1	64	135

2.3 Geophysical data

The most common way to get orientations of the joints in boreholes is through geophysical investigations with sondes. For this project, two types of borehole-wall imaging methods were applied, namely acoustic (ATV) and optical televiewer (OTV) imaging. These two imaging methods can provide continuous and orientated 360° images of the borehole-wall, from which the character and orientation of lithological and structural features can be defined (Williams & Johnson, 2000). As can be seen in figure 2.2 and 2.3, the 360° measurements of the borehole are then projected onto a planar surface. The position of the maximum amplitude defines the dip direction (DD). The dip angle can be calculated with formula 2.1

$$\text{dip} = \tan^{-1}\left(\frac{\text{amplitude}}{\text{diameter}}\right). \tag{2.1}$$

The strike can be calculated with formula 2.2.

$$\text{strike} = \text{DD} - 90°. \tag{2.2}$$

Optical televiewers scan the borehole-wall with a camera and can extract a 360° "photography" of the borehole. With this image (Figure 2.2), the geophysicists can identify single joints, their dip and dip direction. The discrimination between rock and joints works through the intensity of the color spectrum.

The main disadvantage of this method is that it can only be applied in boreholes, which are not filled with water or mud. Another problem are residuals of the drilling liquids at the borehole-wall, which make an identification of discontinuities impossible.

The main advantage of OTV compared to ATV is a clearer distinction between specific dis-

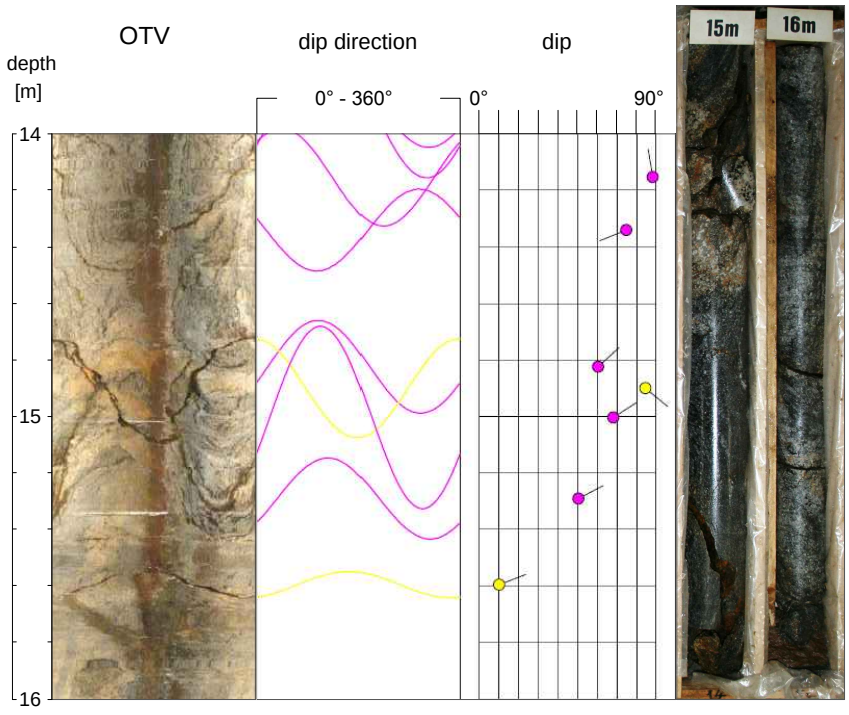

Figure 2.2: Image from the optical televiewer, evaluation of joint orientation and picture of the core sample from the same depth.

continuities and structures of less geomechanical significance, like foliation. It is also possible to define the fraction opening and the filling of a joint.

Acoustic televiewers, which are commonly in use, work with ultrasonic signals. ATV data can also be gained in water– or slightly mud–filled sections of boreholes. Various structures at the borehole-wall like joints, foliation or faults scatter energy of the acoustic beam and reduce the incoming signal. Thus, a contrast between the intact rock and the discontinuities is visible on the images (Paillet et al., 1990).

Conventional ATV systems use an ultrasonic pulse–echo configuration with a 0.5 MHz – 1.5 MHz transducer. This transducer is rotating on a motor–driven shaft while the tool is pulled up–hole (Williams & Johnson, 2004). The identification of certain structures in the borehole is possible due to different acoustic impedances of the rock and the structures. The main problem with this method is the lack of possibility to differentiate between fractures and foliation or bedding planes.

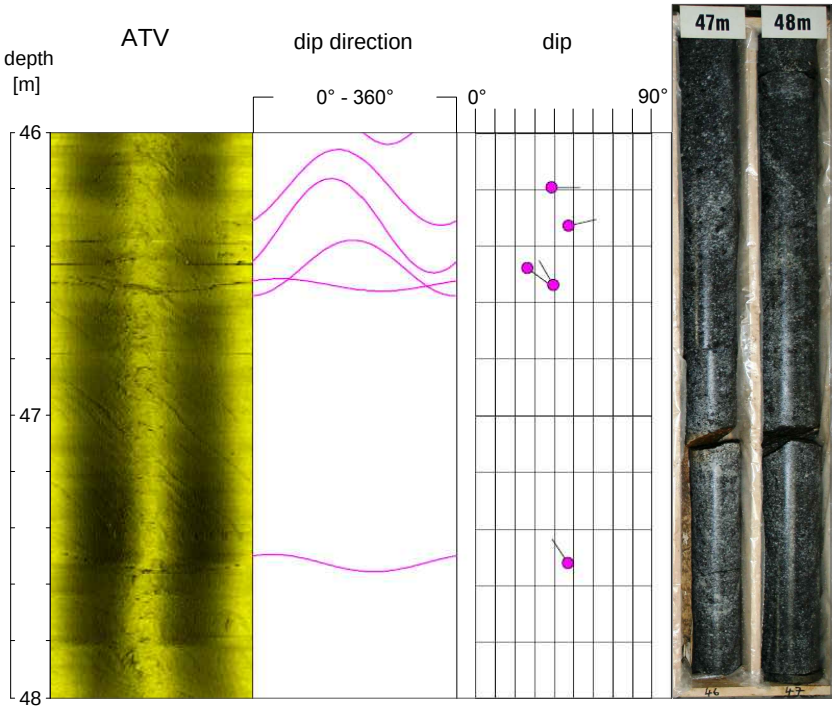

Figure 2.3: Image from the optical televiewer, evaluation of joint orientation and picture of the core sample from the same depth.

3 Methodology

For the description of the different methods of this work, one can distinguish the following groups:

- Evaluation of the provided subsurface data for numerical modeling,
- Field measurement at the surface,
- numerical modeling with 3DEC and
- analytic calculations.

3.1 Field measurement

The fact that the investigated drilling-area is located close to the surface (10 m to 40 m) rises the question if there exists any connection of the surface block size distribution to the subsurface block size distribution. To analyze this issue, measurements of block sizes were evaluated that had been taken across the surface of the project area. All measurements were taken by hand with manual measuring instruments like yardsticks and under the simplified assumption of rectangular blocks, such that sorting of the data in length, width and height could be done afterwards. The measurements are divided into different rock objects (see figure 3.1), namely

- fallen blocks,
- dry-stone wall rocks,
- deposits and
- bedrock.

It is furthermore safe to assume that the dry stone walls, which have served as early protection from rockfall for the local infrastructure, were built from deposit blocks of the nearby

(a) Fallen rocks

(b) Dry-stone wall

(c) Deposit

(d) Bedrock

Figure 3.1: Different types of measured rocks at the surface.

environment.

Because of additional decomposition due to the erosion processes, it is very likely that fallen rocks and deposits cannot represent the *in situ* block size distribution. It is also sure that just the bedrock itself does not represent the subsurface *in situ* block size distribution, as smaller blocks are rarely elements of rock faces at outcrops and would thereby not be represented in the distribution.

The mean block size of the bedrock and the mean block size of the decomposed rock can therefore be expected as extreme values of the actual *in situ* block size distribution, that will lie somewhere in between.

3.2 Evaluation of geophysical measurements

The main challenge when evaluating of the described geophysical measurements is to distinguish between fractions and other detected structures in the borehole. As already mentioned

(section 2.3), discrimination only on the basis of ATV- or OTV-data is not possible. For this reason, it is necessary to compare the measurements with the drilling core sample, where every single discontinuity should be visible. The depth and the dip of a joint can be directly gauged at the core. To determine the dip direction, it is necessary to associate a geophysical measurement with equal depth and equal dip to the core data.

With this procedure, 150 discontinuities were determined in the three boreholes. Figure 3.2 shows all poles of the joints in the *Schmidt net*. All gathered discontinuities are either joints or foliation. The foliation is orientated approximately between 50° to 105° and are overlayed with joints. Faults and slickensides do not occur in the investigated area.

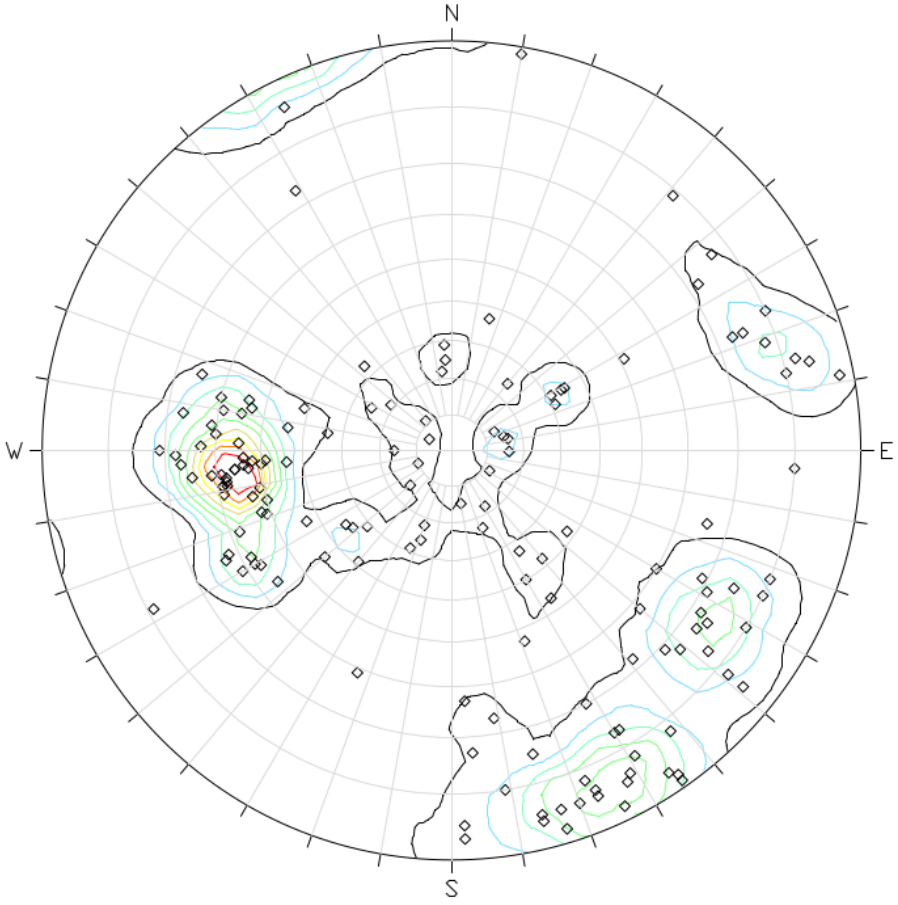

Figure 3.2: Stereonet with all 150 discontinuities, obtained with borehole measurements and drill core sampling.

3.3 DFN modeling

To be able to compare different DFN approaches, different types of 3D models were created. The first model is a deterministic fraction model, the second and third ones are stochastic fraction models. The discontinuities for all these three models are considered completely persistent, because it is not possible to gain valid values of the persistence for the deterministic model from borehole data. A stochastic fraction model with non-persistent discontinuities (values estimated for each set) was furthermore created (see section 3.3.4) to come even closer to the real *in situ* block size distribution and for comparison with the results of the field measurements.

To build the models, 3DEC 5.0 (3-dimensional distinct element code, software of Itasca Consulting Group Inc.) was used. Either each single discontinuity is defined individually, which we did for the deterministic model, or a stochastic model is built with statistical joint set information (Itasca Consulting Group Inc., 2013).

For each of the 3DEC models, the *jset* command was used, with which single joints or sets of joints within a defined volume can be generated. To avoid artificially small block volumes, a minimum block side length was set, which corresponds to the minimum block side length measured at the surface.

3.3.1 Model 1 (deterministic)

The first model serves as a reference model for all other investigations. For this model, every single discontinuity was generated individually in the following way: From the geophysical measurements, one is able to obtain the orientation of each joint that intersects the borehole, and knowing the drill direction and depth, the exact position in space was determined. The actual *in situ* block size distribution can therefore be assumed as well reproduced. Figure 3.3 shows the flow chart for the 3DEC modeling, the entire code is shown in listing 5.1 in the appendix.

As input data, the following parameters for each of the 150 joints were used (see appendix, table 5.1):

- dip angle
- dip direction
- x-, y- and z-coordinates of the intersections with the borehole

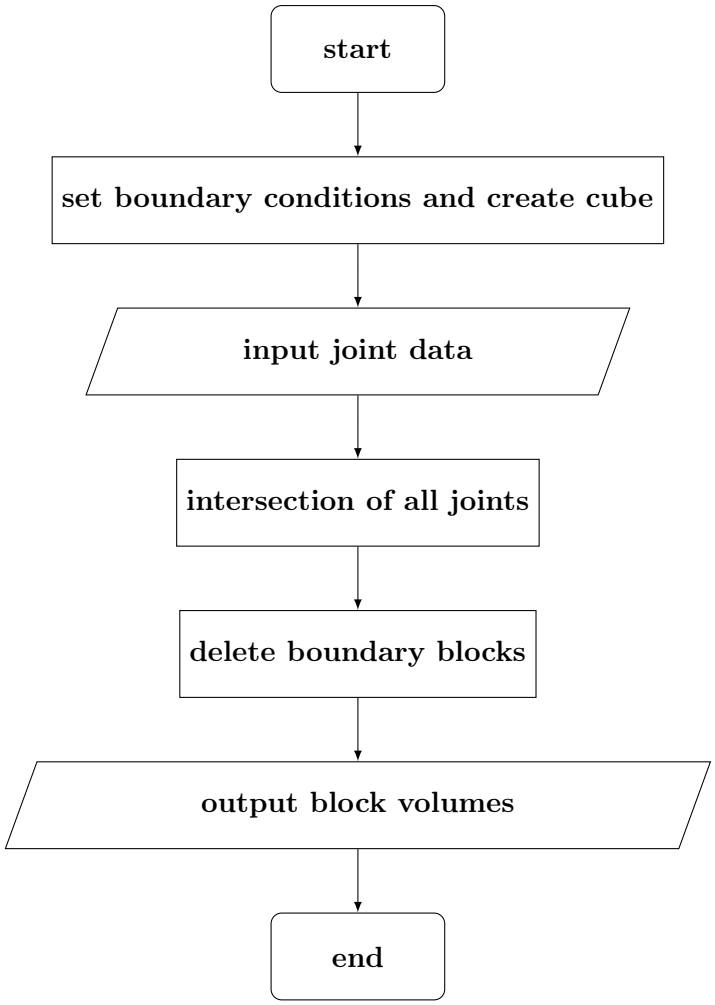

Figure 3.3: Flow chart for 3DEC modeling.

In a first step, the program intersected all discontinuities with each other within a cube of the dimensions 40 m x 40 m x 40 m. This cube size was chosen to be able to cut out cubes of different sizes at a later stage.

As can be seen in figure 3.4, the model still contains blocks at the boundary of the cube, that are not only cut by discontinuities, but also by the model boundary faces itself and are therefore of artificial origin. While not slicing the cube once more but removing these so-called *boundary blocks* (Söllner, 2014) (see figure 3.5), in seven consecutive steps, we gain seven different sets of data, which can later be used to evaluate the influence of the model volume on the block size distribution. Therefore all blocks within a certain range from the cube boundary to 2.5 m (5 m, 7.5 m, ..., 17.5 m respectively) had been deleted on each side of the cube.

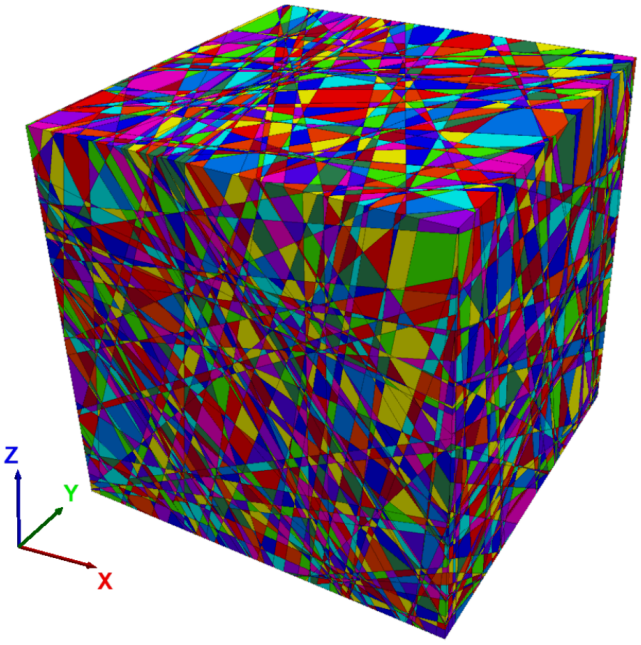

Figure 3.4: Model 1 – cube of 40 m length, still containing boundary blocks.

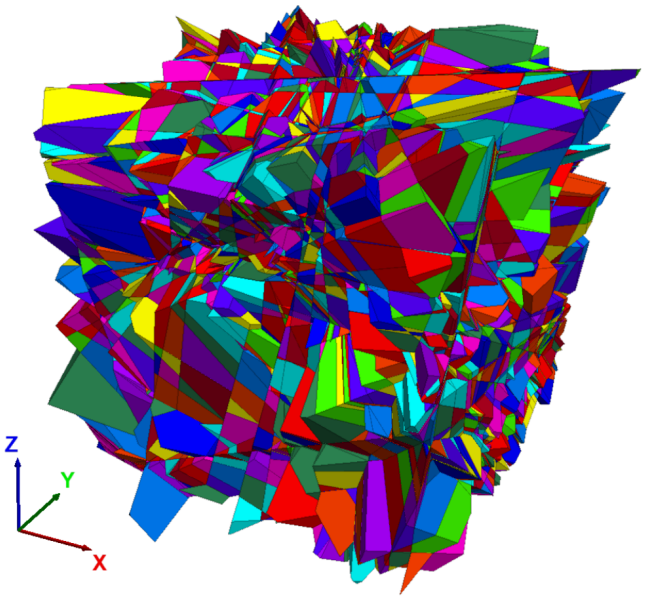

Figure 3.5: Model 1 – cube of 20 m length with deleted boundary blocks.

3.3.2 Model 2 (stochastic, five joint sets)

The second model considers the measured data in a way that is common for typical geotechnical approaches, namely in terms of certain numbers of joint sets and additional arbitrary joints that are not associated with any set. The joints of Model 1 were grouped, such that five sets of joints were determined, which belong to the same family with respect to their orientation, see figure 3.6, and table 3.1 for all 3DEC joint set input parameters, with S for spacing and SD for standard deviation.

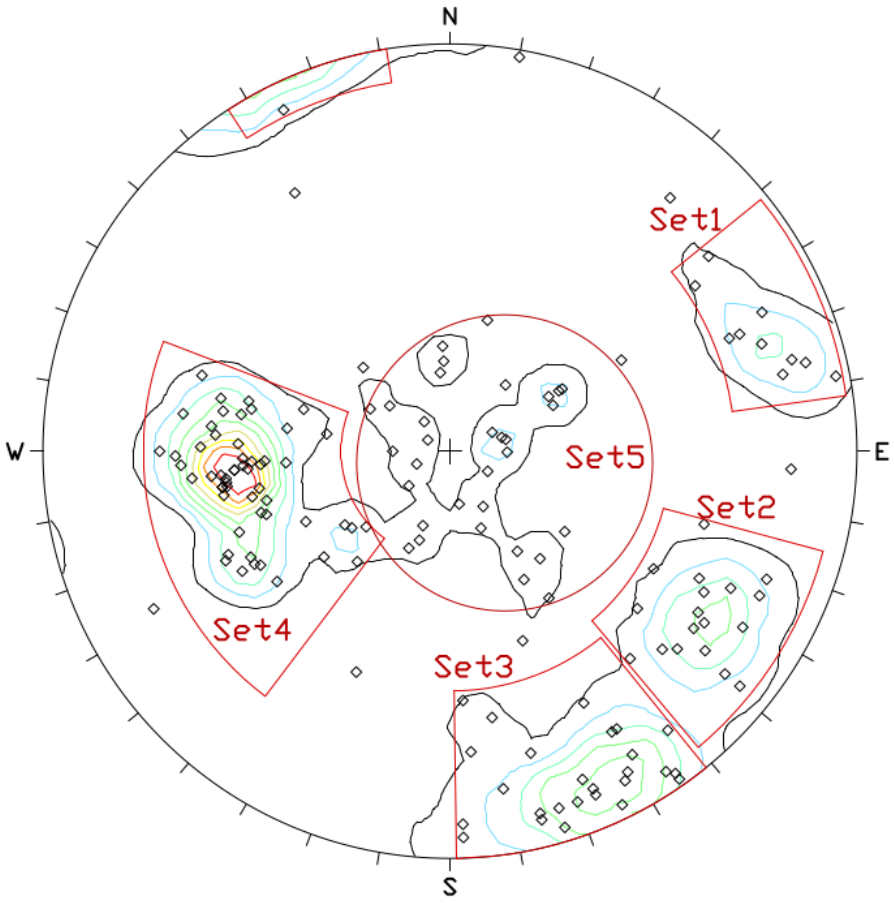

Figure 3.6: Model 2 – stereonet; grouping to five sets.

The additional arbitrary joints that do not fit in the clustering scheme are neglected for the computation of the set orientation statistics. To use the complete data for the calculation of the spacing, however, each of these *off-set joints* were later associated to the best matching set and evaluate the spacings statistically for each set. In general, the measured spacings from the core have to be corrected by a factor of $\cos\beta$, with the dip-angle β, to get the true spacing. As outliers strongly influence the arithmetic mean, the median value of the joint

Table 3.1: 3DEC input parameters for Model 2 with S for spacing and SD for standard deviation.

Set	Dip [°]	Dip_{SD} [°]	DD [°]	DD_{SD} [°]	S_{median} [m]	S_{SD} [m]
Set 1	79	4.97	249	8.66	0.86	1.17
Set 2	73	6.68	303	8.31	0.91	2.94
Set 3	82	6.89	339	37.35	0.50	0.62
Set 4	53	9.03	81	16.53	0.52	3.31
Set 5	6	10.10	278	102.86	2.46	2.46

spacing was used as input parameter. In figure 3.7 statistical values for the spacing of each joint set are shown (for whole spacing data see appendix table 5.2).

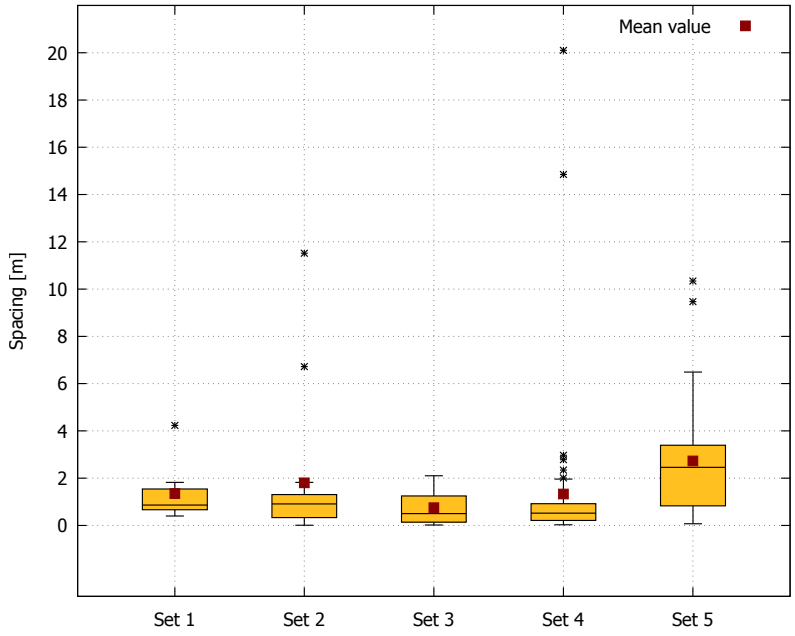

Figure 3.7: Box plot for the spacing of each joint set of Model 2, with outliers and mean values.

Following this procedure, it is possible to simulate block models with five joint sets with values for the orientation and one value for the spacing, respectively. Note that in 3DEC, when the standard deviation is entered additionally, values for the orientation and spacing are randomly generated. The cube of 40 m length with boundary blocks is shown in figure 3.8 and the cube of 20 m length without boundary blocks in figure 3.9.

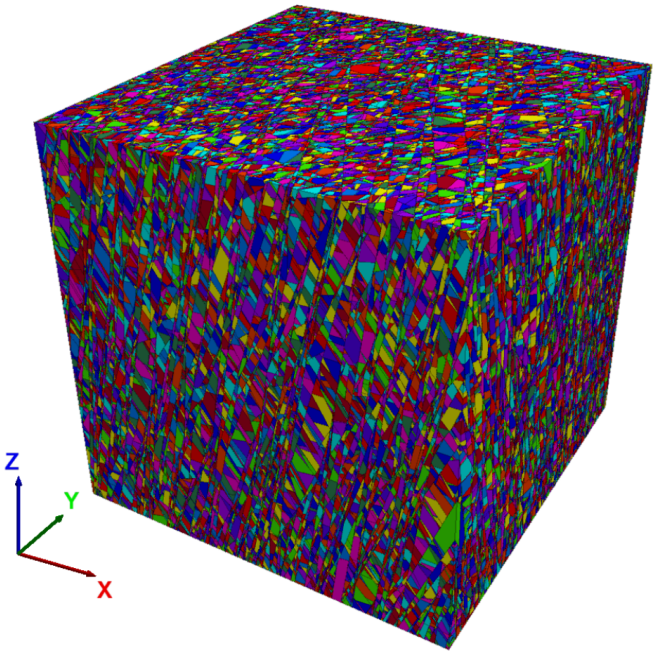

Figure 3.8: Model 2 – cube of 40 m length, still containing boundary blocks.

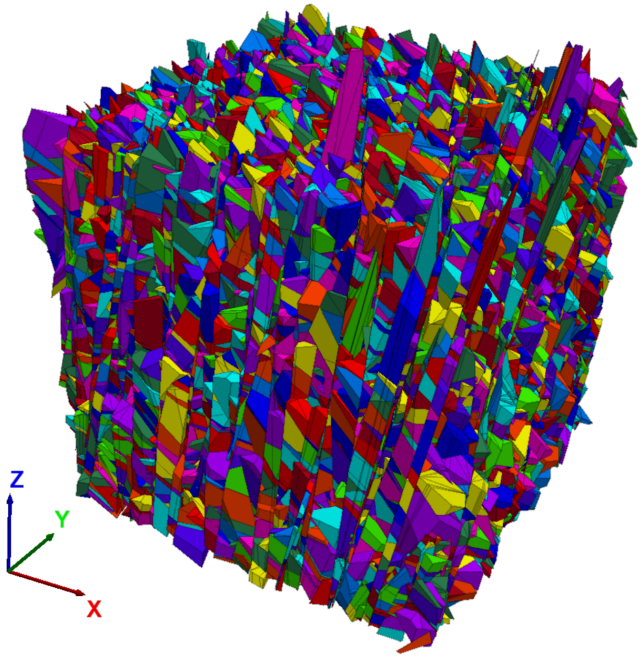

Figure 3.9: Model 2 – cube of 20 m length with deleted boundary blocks.

3.3.3 Model 3 (stochastic, three joint sets)

In order to compare the models with the results of analytic methods that rely on three joint sets only, such as equation 1.4 after Palmström (section 1.1.1), the number of joint sets was restricted to three. This classification is purely artificial and requires further analysis of the data with respect to the geologically heterogeneous nature. Therefore, crucial points in the data were selected that could represent each set well and tested all possible resulting combinations. Due to this so-called *sensibilisation* of the set orientation, an extra diversification of the orientation by the standard deviation, as in Model 2, is not necessary. In figure 3.7 the clustering of the sets and the crucial points are shown in the stereonet.

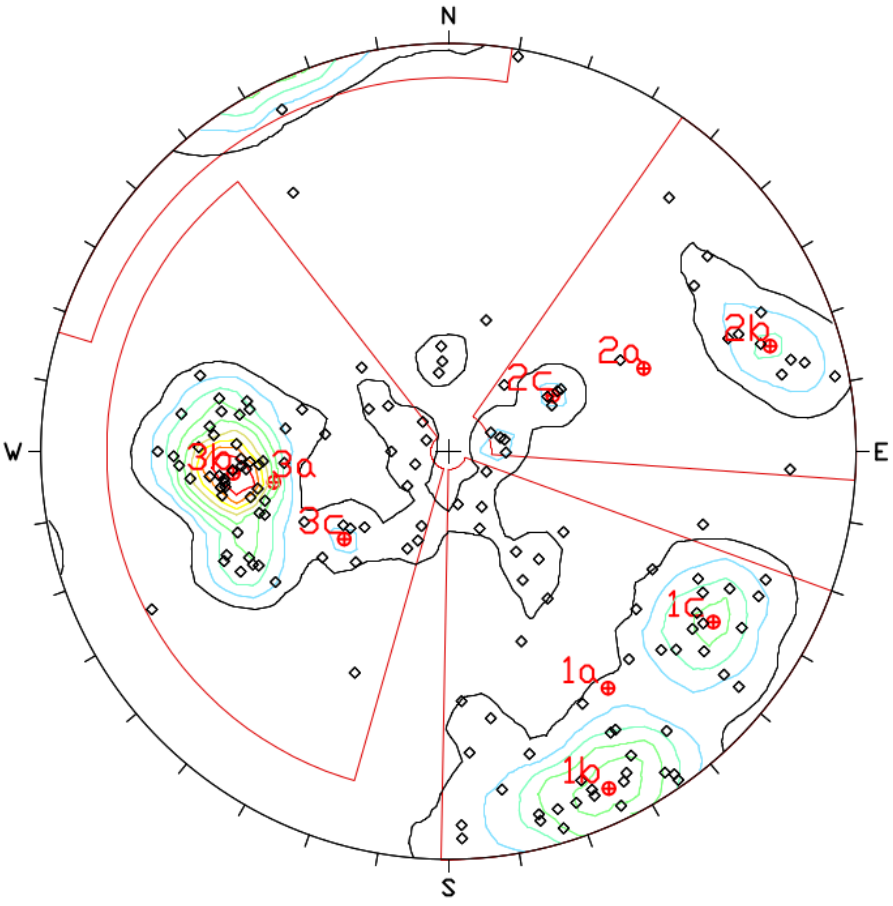

Figure 3.10: Model 2 – stereonet; grouping to three sets with statistical orientation of the clustering (named “a”) plus crucial points (named with “b” and “c”).

The determination of the spacing for Model 3 was done in the same way as for Model 2 (section 3.3.2), but had to be performed for all nine set-points (1a–c, 2a–c, 3a–c) separately,

because different dip angels lead to different spacings. As for Model 2, the spacing shows an asymmetric probability distribution, so the median value as reference value for the spacing was chosen (see figure 3.11 and for the whole spacing data see appendix table 5.3).

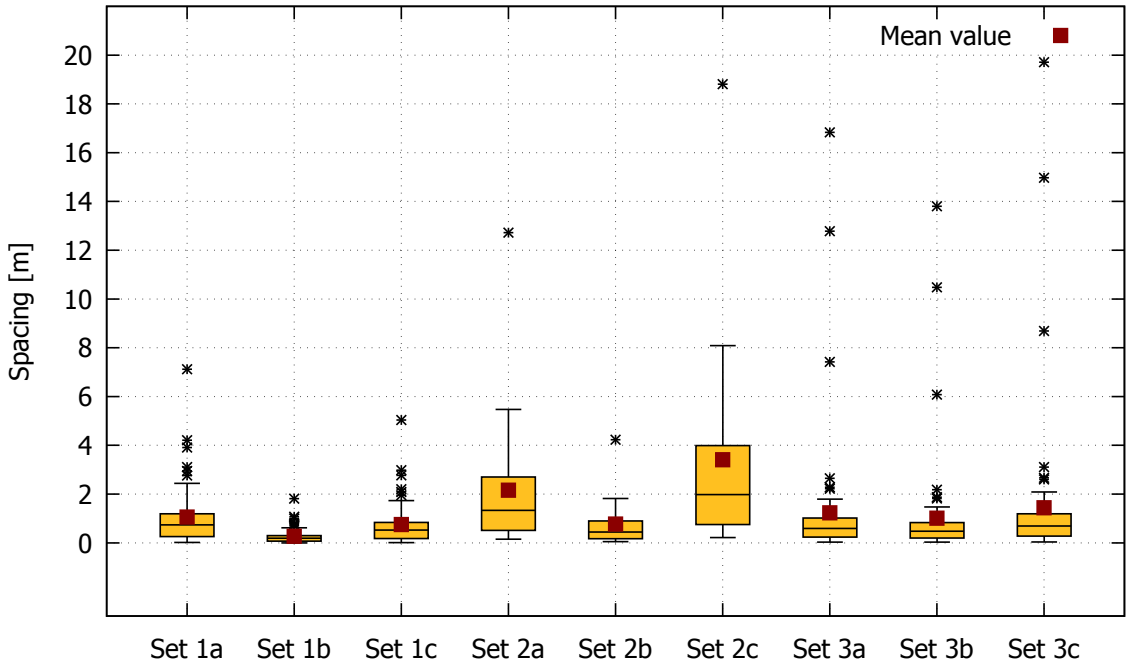

Figure 3.11: Box plot for the spacing of each joint set of Model 3, with outliers and mean values.

Table 3.2 summarizes the resulting joint set parameters for Model 3. Finally, 27 models were generated by combining each set orientation with each other. As explained for Model 2, a cube of 40 m side–length was first built(figure 3.12) and then remove all boundary blocks to get cubes of 20 m side–length (figure 3.13). An additional grading of the cube size, as done for Model 1 and Model 2, was not applied at Model 3, since the influence of the cube size on the block size distribution can already be investigated in great detail with the two previous models.

Table 3.2: 3DEC input parameter for all different joint sets of Model 3 with S for spacing and SD for standard deviation.

Set	Dip [°]	DD [°]	S_{median} [m]	S_{SD} [m]
Set 1a	70	326	0.74	1.28
Set 1b	85	334	0.19	0.33
Set 1c	76	303	0.52	0.92
Set 2a	55	247	1.34	2.79
Set 2b	79	252	0.45	0.93
Set 2c	32	242	1.98	4.12
Set 3a	47	80	0.59	2.65
Set 3b	56	84	0.48	2.17
Set 3c	37	50	0.69	3.10

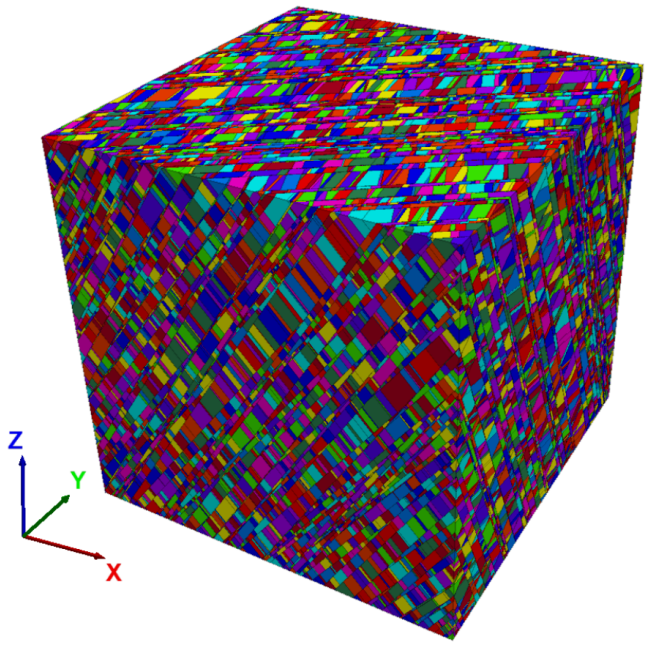

Figure 3.12: Model 3 – cube of 40 m length, combination *aaa*, still containing boundary blocks.

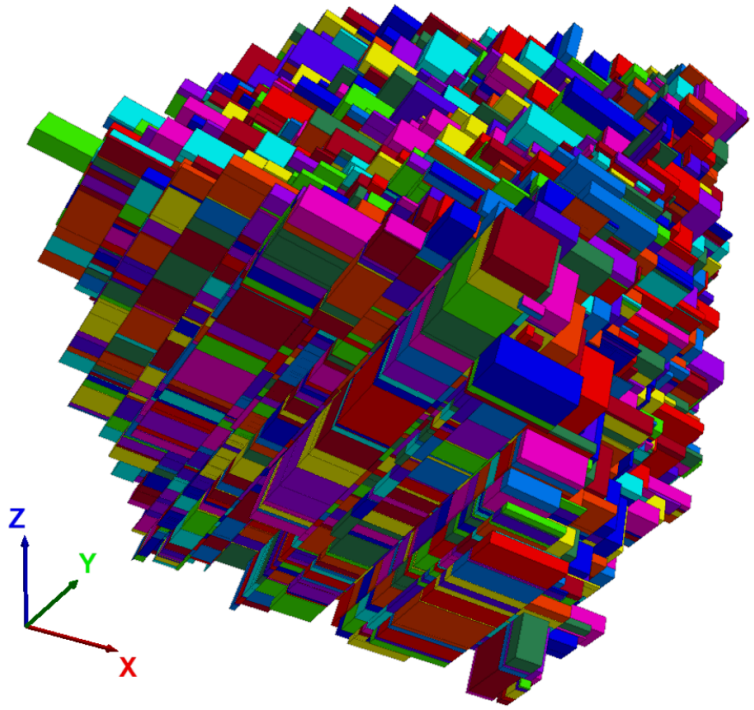

Figure 3.13: Model 3 – cube of 20 m length, combination *aaa*, with deleted boundary blocks.

3.3.4 Model with non–persistent joints (stochastic, five joint sets)

For the sake of completeness, a model with non-persistent joints was also accomplished. For this purpose the input data of Model 2 was used and supplemented by the values for the persistence to each joint set. Table 3.3 shows all input values for the modeling with non-persistent joints.

The values for the persistence (P) refer to a rough estimation of the project geologist, which can only be achieved for actual joint sets. For this reason it is only possible to operate with the data of Model 2, but not with the data of Model 3, because of its artificial joint set clustering.

Moreover, the results of the non-persistent model can only be compared to the results of the field measurements, since the other models consider all discontinuities with full persistence.

The modeling itself was executed in the same way as for Model 2, starting with a cube with the dimensions 40 m x 40 m x 40 m (figure 3.14) and then removing all boundary for different cube sizes (figure 3.15).

Table 3.3: 3DEC input parameter for non–persistent modeling with joint set parameter of Model 2 plus persistence (P).

Set	Dip [°]	Dip_{SD} [°]	DD [°]	DD_{SD} [°]	S_{median} [m]	S_{SD} [m]	P [-]
S 1	79	4.97	249	8.66	0.86	1.17	0.25
S 2	73	6.68	303	8.31	0.91	2.94	0.90
S 3	82	6.89	339	37.35	0.50	0.62	0.90
S 4	53	9.03	81	16.53	0.52	3.31	0.50
S 5	6	10.10	278	102.86	2.46	2.46	0.30

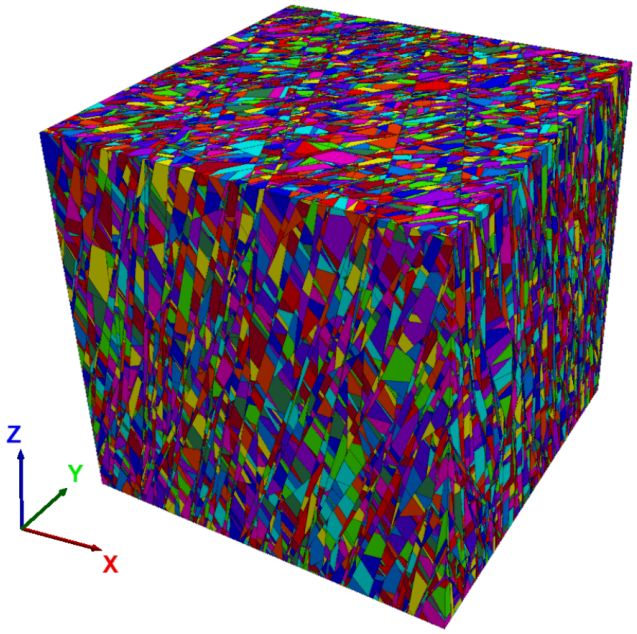

Figure 3.14: Model with non–persistent joints, cube of 40 m length, still containing boundary blocks.

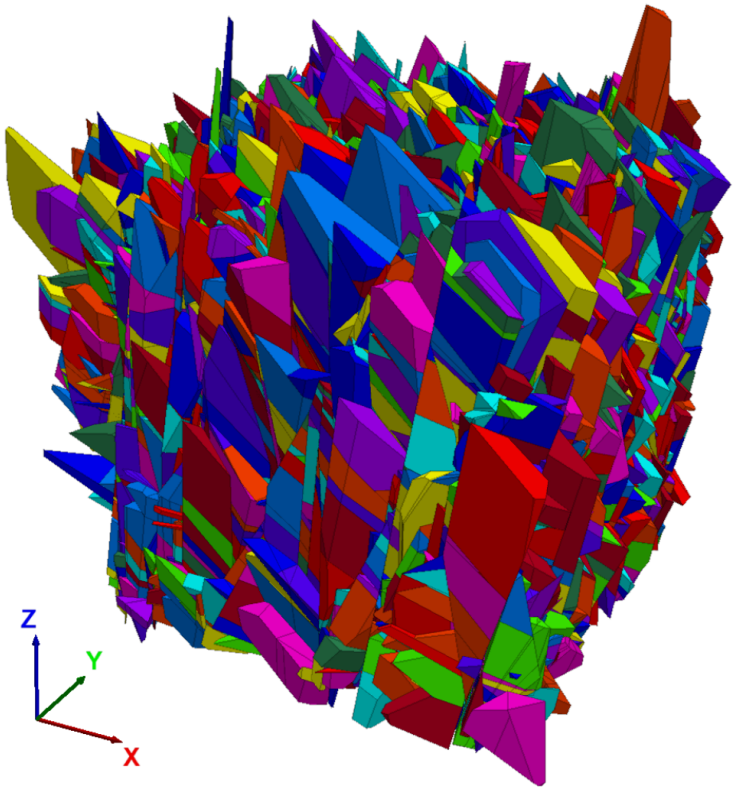

Figure 3.15: Model with non–persistent joints, cube of 20 m length, without boundary blocks.

3.4 Analytic Formula

In order to evaluate an analytic calculation of our example, all combinations of Model 3 were calculated (section 3.3.3) with the formula of Palmström (formula 1.4):

$$V_b = \frac{S_1 \cdot S_2 \cdot S_3}{\sin\gamma_1 \cdot \sin\gamma_2 \cdot \sin\gamma_3}.$$

The other formulae of section 3.3.3 were not used, because they contain parameters for the persistence, which is not available for the three–set model.

The calculations were done in three different ways to allow for a direct comparison of different levels of abstraction.

In the first and most simple case, **Case 1**, a single value for the volume was computed(V_b) with the median of the spacings (S_i) and the intersection angles (γ_i) between each joint set (see figure 1.2). This case should represent the situation where only single values for the

spacing and the orientations are available. All input values for this "standard" computation are listed in table 3.4.

In Case 1, the restriction to the median values of each set is artificial, since it is in general possible to compute each combination of the whole population of spacing values (provided by the core measurements, see appendix table 5.3) separately, with very little numerical effort.

For the S_i in **Case 2**, each measurement of each of the three sets was multiplied with each measurement of the other sets in three nested loops (see Matlab code in listing 3.1), which generated a number of 77220 block volumes that can be treated as a distribution for further analysis.

Listing 3.1: Matlab code for Palmström's formula with whole population of spacing data.

```
i1 = size(Set_1a,1);
j2 = size(Set_2a,1);
k3 = size(Set_3a,1);

l = 1;
for i=1:i1
  for j=1:j2
    for k=1:k3
      V(l) = Set_1a(i) * Set_2a(j) * Set_3a(k);
      l = l+1;
    end
  end
end

gamma = [70.; 79.; 87.];
gamma = gamma / 180. * pi;
gam = sin(gamma(1)) * sin(gamma(2)) * sin(gamma(3));
V = sort(V / gam);
```

In addition a more realistic case was investigated, **Case 3**, for the situation when the whole population of data is not available and one has to rely on statistical values. For this calculation, each set of spacings (S_i) was fitted with a gamma distribution (D_i) with distinct parameters and then generated $n = 10000$ random values (Monte–Carlo Simulation) that follow D_i.

Afterwards, block volumes were generated in such a way that all 27 combinations of Model 3 were computed (n times three nested loops over the S_i's, for computational details see listing 3.2).

Listing 3.2: Matlab code for Palmström's formula with randomly generated spacing data.

```
l=1;
for i=1:3
  for j=1:3
    for k=1:3

                s1 = Set_1a;
                s2 = Set_2a;
                s3 = Set_3a;

                g1 = gamfit(s1);
                g2 = gamfit(s2);
                g3 = gamfit(s3);

                m=1000;
                for ii=1:m
                        V(ii) = gamrnd(g1(1),g1(2),1) * gamrnd(g2(1)
                        ,g2(2),1)
                        * gamrnd(g3(1),g3(2),1);
                end

                gam = sin(ga1(l)) * sin(ga2(l)) * sin(ga3(l));
                V = sort(V / gam);

                l = l + 1;
                fprintf()
    end
  end
end
```

Table 3.4: Input parameters for calculation with Palmström formula.

Combination	S_1 [m]	S_2 [m]	S_3 [m]	γ_1 [°]	γ_2 [°]	γ_3 [°]
aaa	0.74	1.34	0.59	70	79	87
aab	0.74	1.34	0.48	70	71	80
aac	0.74	1.34	0.69	70	89	71
aba	0.74	0.45	0.59	71	54	87
abb	0.74	0.45	0.48	71	46	80
abc	0.74	0.45	0.69	71	67	71
aca	0.74	1.98	0.59	70	78	87
acb	0.74	1.98	0.48	70	86	80
acc	0.74	1.98	0.69	70	69	71
baa	0.19	1.34	0.59	85	79	82
bab	0.19	1.34	0.48	85	71	76
bac	0.19	1.34	0.69	85	89	78
bba	0.19	0.45	0.59	81	54	82
bbb	0.19	0.45	0.48	81	46	76
bbc	0.19	0.45	0.69	81	67	78
bca	0.19	1.98	0.59	87	78	82
bcb	0.19	1.98	0.48	87	86	76
bcc	0.19	1.98	0.69	87	69	78
caa	0.52	1.34	0.59	54	79	69
cab	0.52	1.34	0.48	54	71	61
cac	0.52	1.34	0.69	54	89	89
cba	0.52	0.45	0.59	50	54	69
cbb	0.52	0.45	0.48	50	46	61
cbc	0.52	0.45	0.69	50	67	89
cca	0.52	1.98	0.59	63	78	69
ccb	0.52	1.98	0.48	63	86	61
ccc	0.52	1.98	0.69	63	69	89

4 Results and Discussion

To be able to compare the results of all measurements, DFN models and calculations, the following statistical parameters are determined:

- Maximum block size (V_{max})
- Mean block size (V_{mean})
- Median of the block size distribution (V_{median})
- Standard deviation of the block size distribution (V_{SD})
- Minimum block size (V_{min})
- Number of single blocks (No.)

Besides the statistical analysis, the entire block size distributions of all 3DEC–models and of the field measurements are illustrated in a cumulative probability graph. The curves follow a log-normal distribution. Additionally, a closer focus was set on the median value to describe the representative block volume of each model.

4.1 3DEC–modeling for non–persistent joints and field measurements

In this section, the results of the field measurements (section 3.1) are related to the results of the numerical model with non–persistent joints of (section 3.3.4). These two data sets are comparable, because both contain the persistence of the rock mass and therefore refer to the actual in *situ* block size distribution as it should appear in nature.

4.1.1 Results of the non–persistent 3DEC–models

The 3DEC–model with non–persistent discontinuities was used to evaluate the entire concept of numerical modeling. One can assume that the block size distribution at the surface strongly correlates with the block size distribution of the investigated rock mass, with some restrictions. Figure 4.1 shows the in situ block size distribution of models with different cube sizes. It is clearly recognizable that in this case the cube size does not have a notable impact on the distribution.

From the statistic values in table 4.1 we can conclude that all values, except the maximum value, are within a close range. We put this down to the fact, that big blocks are statistically rare and have appeared in ranges, which were deleted later to cut out the required cube sizes. Thus the model with the largest cube size also contains the largest block size.

It should also be noted, that the for this model, the in situ block size distribution strongly depends on the values for the persistence.

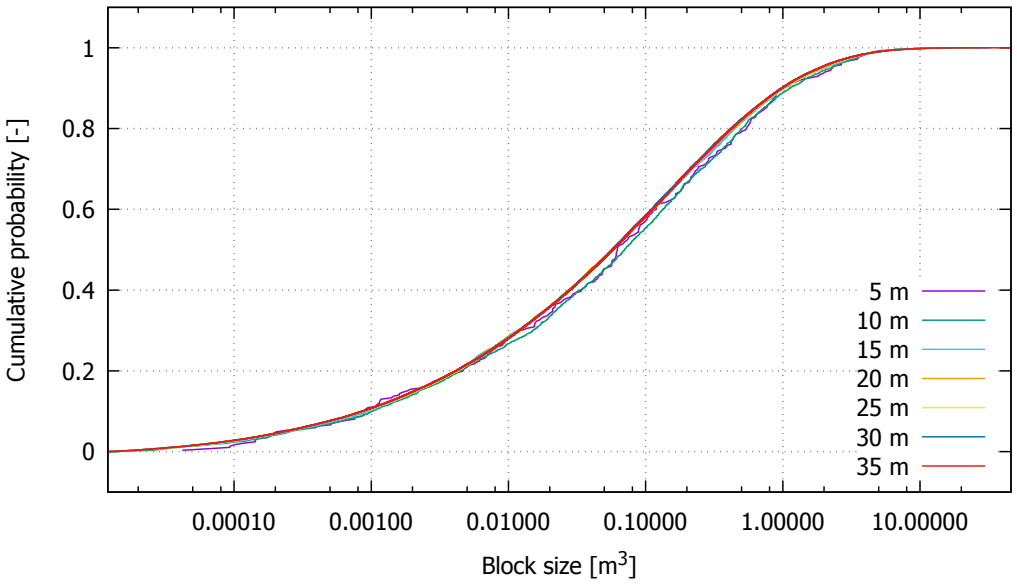

Figure 4.1: In situ block size distribution of non–persistent joint model with different cube sizes.

Table 4.1: Statistic values for the block volume of the non–persistent joint models (see section 3.3.4).

Cube length	V_{max} [m^3]	V_{mean} [m^3]	V_{median} [m^3]	V_{SD} [m^3]	V_{min} [m^3]	No. [–]
5	13.41	0.457	0.062	1.21	4.19E-05	285
10	22.57	0.435	0.070	1.10	1.23E-05	2,309
15	27.42	0.403	0.057	1.08	1.22E-05	8,338
20	27.42	0.397	0.057	1.07	1.21E-05	20,025
25	27.42	0.396	0.057	1.07	1.20E-05	39,395
30	32.20	0.387	0.057	1.06	1.20E-05	69,756
35	46.06	0.389	0.058	1.07	1.20E-05	110,248

4.1.2 Results of field measurements

In figure 4.2, cumulative probability curves of the block volumes of each different rock type measured in the field (section 3.1) are plotted. Additionally, we added the curve of the non–persistent model with 20 m cube length for comparison. The figure shows that the distribution of the numerical model comes reasonably close to the distribution of the outcrop.

A larger deviation can be observed at smaller block volumes. The reason for this deviation is that small blocks rarely remain at rock faces and are more prone to erosion, thus the small blocks are then under–represented in the curve of the blocks measured at outcrops (bedrock) and are over–represented in the curves of the other measured rock types, that contains eroded objects.

When comparing the statistic values of the 3DEC–model with the statistic values in table 4.2 for the surface objects, it is furthermore obvious that the maximum bedrock volume is much lower. The reason for this is that extreme large blocks are very rare at outcrops. Even if a very large outcrop is available, it is unlikely to show non–eroded large blocks.

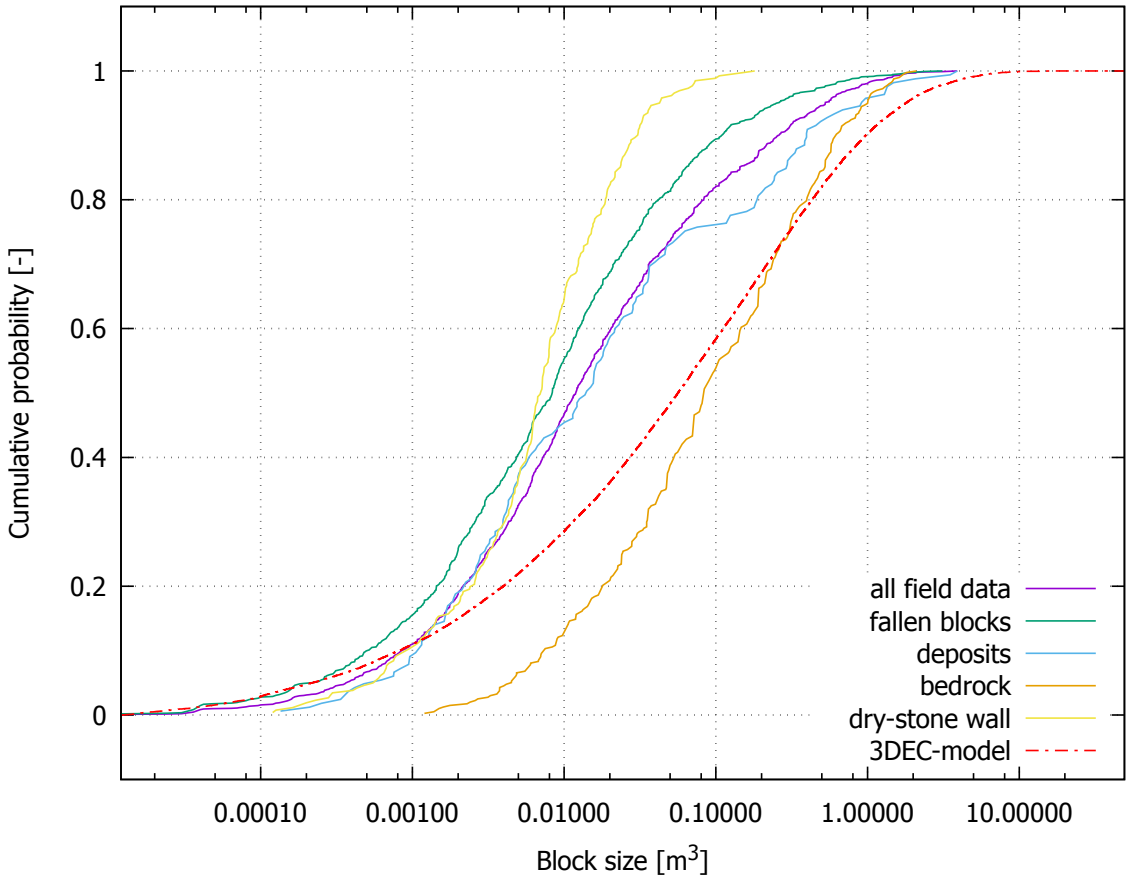

Figure 4.2: Cumulative probability distribution for the field measurements and for the numerical non–persistent model with 20 m cube length (section 3.3.4).

Table 4.2: Statistic values for block volumes determined with field measurements.

Objects	V_{max} [m^3]	V_{mean} [m^3]	V_{median} [m^3]	V_{SD} [m^3]	V_{min} [m^3]	No. [–]
all	3.90	0.099	0.012	0.28	1.20E-05	1,900
fallen blocks	3.12	0.059	0.008	0.21	1.20E-05	1,077
deposits	3.90	0.173	0.014	0.49	1.35E-04	165
bedrock	2.10	0.236	0.084	0.34	1.20E-03	397
wall rocks	0.18	0.013	0.007	0.02	1.20E-04	261

4.2 3DEC–modeling with persistent joints

4.2.1 Results – Model 1 (deterministic)

At the first sight, the outcome of the deterministic model (figure 4.3) shows greater scattering for different cube sizes compared to the outcome of the model with non–persistent discontinuities (figure 4.1). This phenomenon is due to the fact that the deterministic input data has a lower level of repetition than the statistic input data.

Also the calculated values (see table 4.3) show some major differences. The maximum volume is noticeable larger than the maximum block sizes of the models with non–persistent joints (see table 4.1), although the model at hand only contains totally persistent discontinuities and therefore the maximum block size should be smaller. The deterministic model contains relatively large blocks, because the joint spacings for the model are not completely homogeneous and partially a large spacing up to several meters occurs (see figure 3.7). The statistical models can not totally reproduce this inhomogeneity and so the maximum block volume of the deterministic model is larger.

It is worth mentioning that the larger volumes of the models with large cube sizes result because for the deterministic model each joint, encountered in one of the boreholes, is just defined once. With increasing cube size, the volume within which no joints are defined increases too. On the other hand, the median also increases from 15 m–cube size to 5 m–cube size, because variations of the input data have an enhanced effect on models with smaller cube sizes featuring less joints.

Table 4.3: Statistic values for the block volume of Model 1.

Cube length	V_{max} [m^3]	V_{mean} [m^3]	V_{median} [m^3]	V_{SD} [m^3]	V_{min} [m^3]	NO. [–]
5 m	6.64	0.251	0.031	0.59	1.66E-05	426
10 m	57.72	0.268	0.025	1.30	1.22E-05	3,707
15 m	57.72	0.226	0.020	1.02	1.22E-05	15,253
20 m	57.72	0.238	0.022	1.01	1.20E-05	33,462
25 m	68.23	0.269	0.025	1.06	1.20E-05	56,638
30 m	74.23	0.332	0.030	1.35	1.20E-05	80,247
35 m	82.11	0.415	0.035	1.77	1.20E-05	103,510

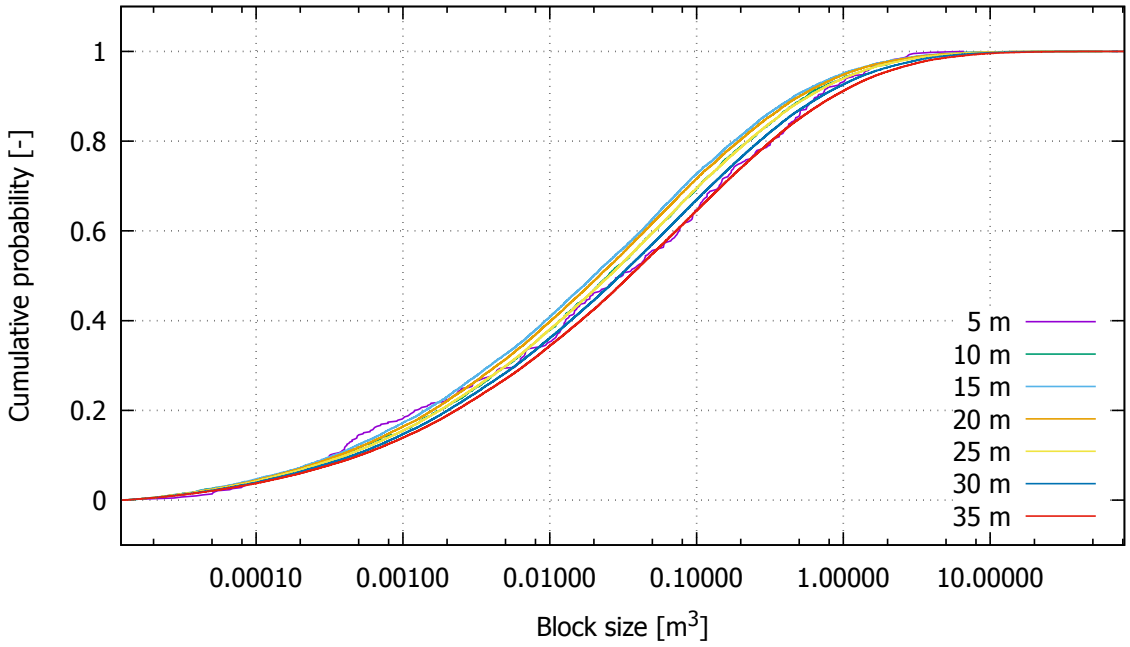

Figure 4.3: In situ block size distribution of Model 1 with different cube sizes.

4.2.2 Results – Model 2 (stochastic, five joint sets)

For the statistic model with fully persistent discontinuities, figure 4.4 shows that the cube size has no influence on the block size distribution. Only the curve for 5 m–cube shows some deviations, also since a curve with less values appears less smooth than the curves for the cube sizes with a higher number of values. It is anticipated that for this approach, the size of the model is variable, as long as the rock mass is more or less homogeneous.

In table 4.4 we can see that the statistic values of all models are very close. Only the maximum block volumes strongly deviate. As already mentioned in section 4.1.1, larger blocks remain in models with bigger cube size, which later on are removed for the models with smaller cube sizes.

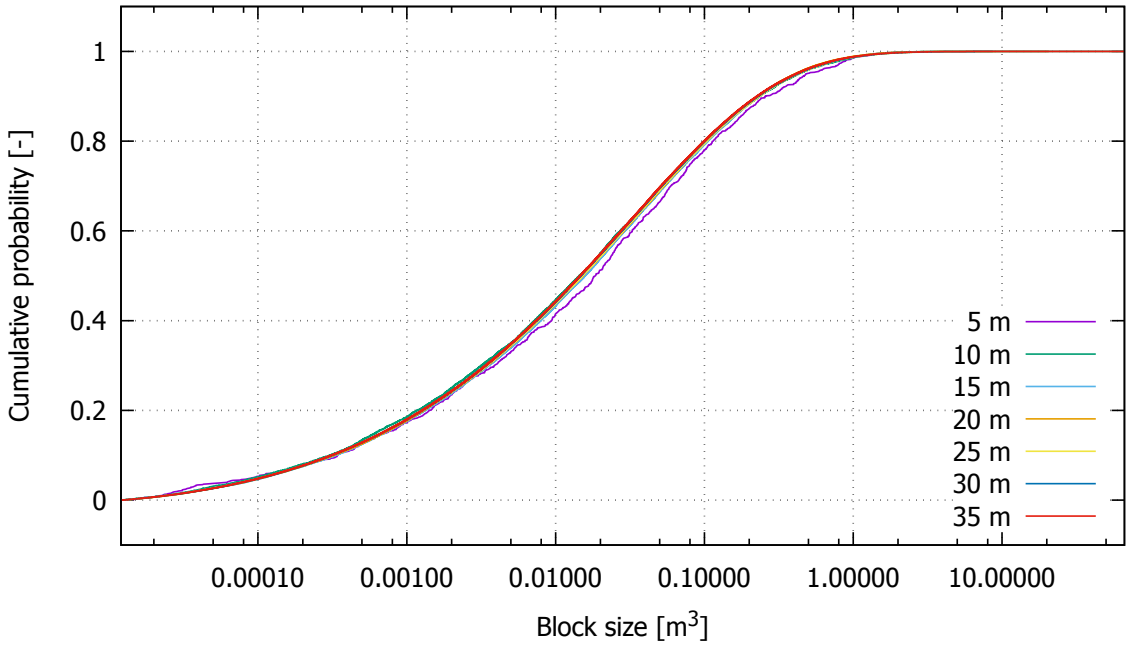

Figure 4.4: In situ block size distribution of Model 2 with different cube sizes.

Table 4.4: Statistic values for the block volume of Model 2.

Cube length	V_{max} [m^3]	V_{mean} [m^3]	V_{median} [m^3]	V_{SD} [m^3]	V_{min} [m^3]	NO. [–]
5 m	8.66	0.108	0.019	0.34	1.43E-05	1,180
10 m	8.66	0.092	0.014	0.25	1.20E-05	10,923
15 m	20.58	0.090	0.016	0.26	1.20E-05	37,231
20 m	20.58	0.088	0.015	0.24	1.20E-05	90,771
25 m	66.43	0.098	0.015	0.44	1.20E-05	160,845
30 m	66.43	0.095	0.015	0.39	1.20E-05	285,622
35 m	66.43	0.092	0.015	0.36	1.20E-05	466,639

4.2.3 Results – Model 3

When looking at the results of Model 3 (figure 4.5), it is apparent that the curves are relatively widespread, although their form (e.g. gradient) is quite similar. In the figure we can see that the dispersion of all curves is not homogeneous. They can be roughly grouped into three sections, differing significantly in their median values. The upper section contains the combinations *bba*, *bbb*, and *bbc*, the middle one *bab*, *bac*, *bcb*, *baa*, *abb*, *cbc*, *cba*, *cbb*, *bca*, *aba*, *abc*, and *bcc*. The lower group consists of *cab*, *aaa*, *cac*, *ccc*, *aab*, *acb*, *caa*, *cca*, *ccb*, *aac*, *aca*, and *acc*. By comparing with the results of the other models, it can be said that the upper group, with the selected set orientation "b" of the clustered joint Set 1 and Set 2 (see figure 3.10), is the closest to the other models.

From the table with the calculated statistic values (table 4.5) one can extract that the difference between the highest (*acc*) and the lowest (*bbb*) median value is more than by a factor of ten. The other statistical parameters show a high dispersion as well, but are relatively homogeneous within the three groups.

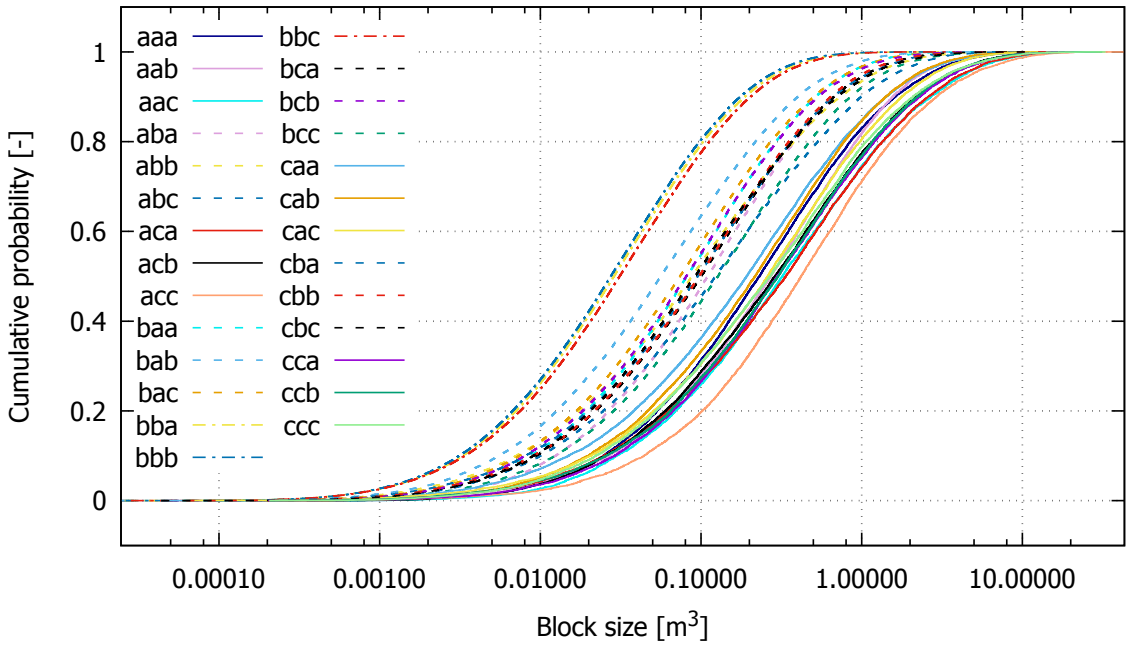

Figure 4.5: In situ block size distribution of Model 3 for different combinations of joint sets.

Table 4.5: Statistic values for the block volume of Model 3 for different combinations of joint sets.

Comb.	V_{max} [m^3]	V_{mean} [m^3]	V_{median} [m^3]	V_{SD} [m^3]	V_{min} [m^3]
aaa	16.43	0.623	0.232	1.11	1.72E-04
aab	15.31	0.619	0.272	1.00	2.92E-04
aac	26.63	1.005	0.322	1.89	4.84E-04
aba	10.94	0.275	0.110	0.49	1.55E-04
abb	13.85	0.276	0.088	0.53	6.44E-05
abc	10.50	0.372	0.123	0.67	8.46E-05
aca	29.65	0.983	0.337	1.84	1.89E-04
acb	19.08	0.834	0.288	1.50	3.51E-04
acc	43.22	1.163	**0.419**	2.20	1.16E-04
baa	5.72	0.202	0.082	0.33	6.26E-05
bab	5.60	0.154	0.056	0.27	2.45E-05
bac	6.59	0.195	0.074	0.35	3.65E-05
bba	3.06	0.073	0.029	0.13	2.59E-05
bbb	2.94	0.069	**0.027**	0.12	2.62E-05
bbc	3.82	0.079	0.031	0.14	2.82E-05
bca	9.62	0.260	0.100	0.45	4.90E-05
bcb	7.53	0.211	0.081	0.37	5.01E-05
bcc	10.76	0.334	0.128	0.60	9.69E-05
caa	21.03	0.870	0.299	1.58	2.02E-04
cab	12.53	0.547	0.217	0.93	1.97E-04
cac	21.23	0.676	0.260	1.18	5.92E-05
cba	7.30	0.262	0.095	0.47	4.35E-05
cbb	14.23	0.253	0.097	0.47	6.25E-05
cbc	11.87	0.274	0.092	0.53	4.37E-05
cca	21.03	0.870	0.299	1.58	2.02E-04
ccb	31.47	0.847	0.302	1.58	2.08E-04
ccc	33.01	0.819	0.270	1.64	2.05E-04

4.2.4 Summary of results of the models with persistent joints

To allow for a direct comparison between Models 1, 2 and 3, representative block size distributions for each model are plotted in figure 4.6: The distributions of Model 1 and Model 2 with 20 m-cube length each, and the upper group of distributions of Model 3.
It is apparent that the block size distribution of Model 2 is close to the one of the deterministic reference model, only in the range of larger block volumes, the curves deviate considerably. However, one can conclude that a simplified DFN–model (Model 2) using statistical joint set parameters, can produce a suitable block size distribution, while keeping in mind that here the geological data was processed in an unusually detailed way.
The distributions of Model 3 deviate significantly from the one of the deterministic model such that the actual block size distribution is poorly reproduced. Therefor one can conclude, that any reduction of naturally occurring joint sets (Model 2: 5 sets > Model 3: 3 sets) is not valid, if the distribution of block sizes is requested.

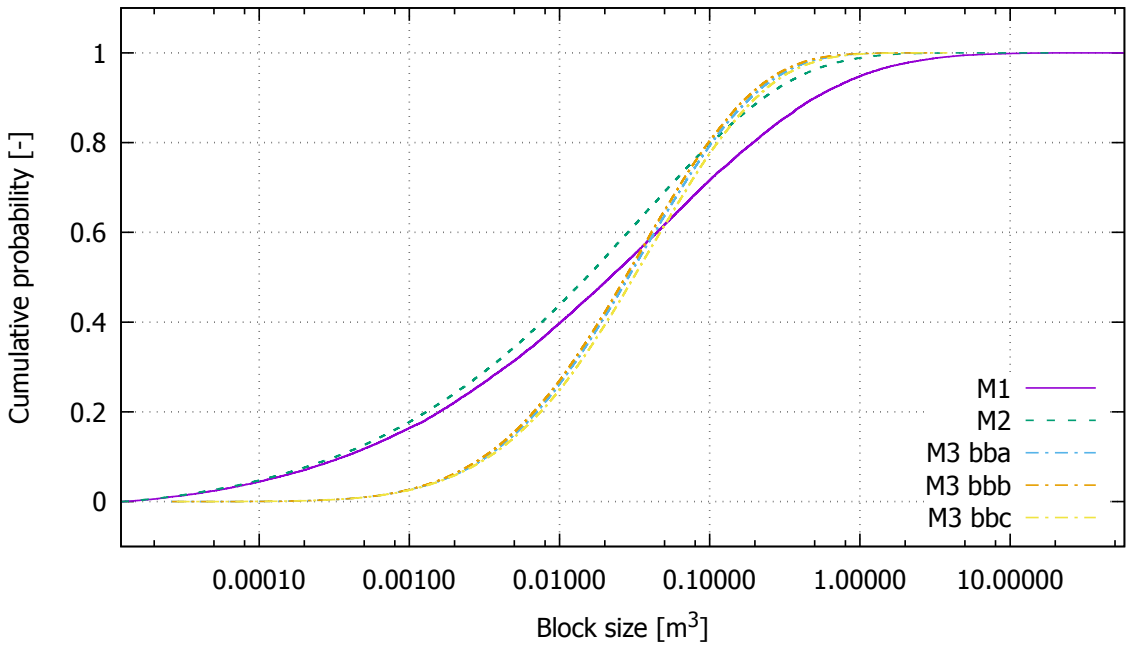

Figure 4.6: Comparison of block size distributions of different models with persistent joints.

A closer look at the statistic values in table 4.6 reveals that, in stark contrast to the distributions, the median values for all three models are close, however not the mean values. At the least the median can be considered as a more representative value for the block size distributions than the mean, which could correspond to the power of three scaling of the volume and thus the overrepresenting of extreme values in the spacings.

In addition one can say that if only a representative volume for the block size distribution is requested, and the median value is used, then even the simplified Model 3 may be adequate. Nevertheless, if such a simplification to three joint sets is done, it is necessary to define representative values for the set orientation manually and not to take the statistic values of the set clustering (here: a-values, compare with figure 3.10).

Table 4.6: Comparison of statistic values for the block volume of Model 1, 2 and 3.

Model	V_{max} [m^3]	V_{mean} [m^3]	V_{median} [m^3]	V_{SD} [m^3]	V_{min} [m^3]	No. [–]
M1	57.72	0.238	0.022	1.01	1.20E-05	33,462
M2	20.58	0.088	0.015	0.24	1.20E-05	90,771
M3 bba	3.06	0.073	0.029	0.13	2.59E-05	109,781
M3 bbb	2.94	0.069	0.027	0.12	2.62E-05	116,762
M3 bbc	3.82	0.079	0.031	0.14	2.82E-05	101,405

4.3 Results of analytic calculations

In the preceding sections, the outcomes of our numerical modeling had been discussed. Now the results of the three cases (section 3.4), computed with the equation of Palmström are compared with each other.

In table 4.7, the results of the standard calculation (Case 1) are listed together with those of Case 2. Although Case 1 was calculated with the median values of the spacings, the results of Case 1 can be considered as a mean block volume. For Case 2 the focus is set on the more plausible median values again. Generally the values of Case 1 are higher than the one of Case 2, with a relative error varying between 38 % and 46 %. In Case 2, the values for V_{max} are inappropriately high, because extreme combinations of spacings are considered as well. The scattering of the median values is comparable to the one of Model 3 (see table 4.5).

Additionally, a Monte–Carlo simulation with fitted gamma distributions for the spacings (Case 3, section 3.4) was performed. The results of these computations are listed in table 4.8. When comparing to the results of Case 2, a relative error occurs between 9 % and 28 %, which reflects rather the varying quality of the respective fit, than the method itself. This reflects e.g. in unreasonable low values for V_{min}, since the gamma distribution has no lower bound for certain sets of input parameters.

Table 4.7: Statistic values of Case 2 compared to the results of Case 1.

Comb.	V_{max} [m^3]	V_{mean} [m^3]	V_{median} [m^3]	V_{SD} [m^3]	V_{min} [m^3]	Case 1 [m^3]
aaa	1,655.20	3.29	0.39	18.83	8.87E-05	0.635
aab	1,428.80	2.84	0.34	16.25	7.66E-05	0.545
aac	2,009.90	3.99	0.47	22.86	1.08E-04	0.772
aba	664.00	1.32	0.16	7.55	3.56E-05	0.255
abb	620.90	1.23	0.15	7.06	3.33E-05	0.236
abc	721.77	1.43	0.17	8.21	3.87E-05	0.280
aca	2,456.00	4.78	0.54	27.84	1.32E-04	0.942
acb	2,002.30	3.90	0.44	22.70	1.07E-04	0.762
acc	3,182.60	6.19	0.70	36.08	1.71E-04	1.225
baa	401.23	0.80	0.09	4.56	2.15E-05	0.155
bab	348.58	0.69	0.08	3.96	1.87E-05	0.134
bac	467.00	0.93	0.11	5.31	2.50E-05	0.181
bba	163.35	0.32	0.04	1.86	8.75E-06	0.063
bbb	153.73	0.31	0.04	1.75	8.24E-06	0.059
bbc	170.20	0.34	0.04	1.94	9.12E-06	0.067
bca	593.89	1.15	0.12	6.73	3.00E-05	0.230
bcb	487.30	0.94	0.10	5.52	2.46E-05	0.186
bcc	737.69	1.42	0.15	8.36	3.72E-05	0.286
caa	1,454.70	2.89	0.34	16.55	7.80E-05	0.551
cab	1,321.70	2.62	0.31	15.03	7.08E-05	0.500
cac	1,561.60	3.10	0.37	17.76	8.37E-05	0.592
cba	620.10	1.23	0.15	7.05	3.32E-05	0.237
cbb	610.37	1.21	0.14	6.94	3.27E-05	0.233
cbc	595.90	1.18	0.14	6.78	3.19E-05	0.230
cca	1,959.80	3.80	0.43	22.21	1.05E-04	0.746
ccb	1,681.80	3.26	0.37	19.06	9.01E-05	0.638
ccc	2,245.10	4.35	0.49	25.45	1.20E-04	0.857

Table 4.8: Statistic values of Case 3 (Monte–Carlo simulation).

Comb.	V_{max} [m^3]	V_{mean} [m^3]	V_{median} [m^3]	V_{SD} [m^3]	V_{min} [m^3]
aaa	826.41	3.48	0.50	14.83	9.18E-08
aab	384.06	2.90	0.42	9.52	2.67E-08
aac	369.59	4.09	0.66	12.95	1.38E-07
aba	80.40	1.28	0.19	3.73	5.75E-08
abb	92.16	1.17	0.17	3.46	1.65E-07
abc	150.27	1.49	0.20	4.92	1.31E-07
aca	325.27	4.72	0.69	14.48	3.22E-08
acb	324.20	3.83	0.59	11.49	6.63E-09
acc	820.57	5.94	0.89	19.63	1.71E-07
baa	269.27	0.81	0.11	4.51	6.46E-08
bab	64.26	0.70	0.10	2.30	1.12E-07
bac	59.02	0.93	0.14	2.85	7.56E-08
bba	24.15	0.32	0.05	0.95	4.30E-09
bbb	30.28	0.30	0.04	0.93	5.60E-11
bbc	35.78	0.33	0.05	1.03	7.83E-09
bca	208.61	1.15	0.16	3.96	7.42E-10
bcb	108.48	0.98	0.13	3.34	6.32E-09
bcc	149.84	1.49	0.19	4.77	2.57E-08
caa	261.14	2.92	0.44	9.11	5.88E-08
cab	514.97	2.58	0.38	10.22	2.91E-08
cac	244.17	3.02	0.46	8.97	1.00E-08
cba	136.03	1.24	0.18	4.08	2.59E-08
cbb	155.31	1.28	0.18	4.56	2.01E-07
cbc	139.81	1.22	0.17	4.12	1.67E-09
cca	297.74	3.69	0.55	10.94	5.74E-08
ccb	533.70	3.28	0.46	11.26	5.00E-11
ccc	363.25	4.22	0.61	12.58	2.93E-08

4.4 GSI for different approaches

To compare the numerical models with the analytic calculations, and to estimate the effect, the different approaches could have on the rock mass characterization, the different results of this work are show on the GSI-chart in figure 4.7. Since the predicted ground type of the investigated area is GT 2 (see table 2.1), the joint conditions are assumed to be of the type "good" (second column of the GSI-chart). In principle all three 3DEC models fall into the category "very blocky", in contrast to the Palmström models with the characterization "blocky", although their margin is small. The reference model (Model 1) shows a GSI-value in the range from 53 to 63, which also almost holds for Model 2, Model 3 and partly for the Palmström cases. Here, Case 1 and Case 3 are located in the range of 57 to 67, whereas Case 2 lies in the range from 55 to 65. In conclusion, it can be stated, that the impact of the different approaches on the rock mass characterization via GSI is relatively low.

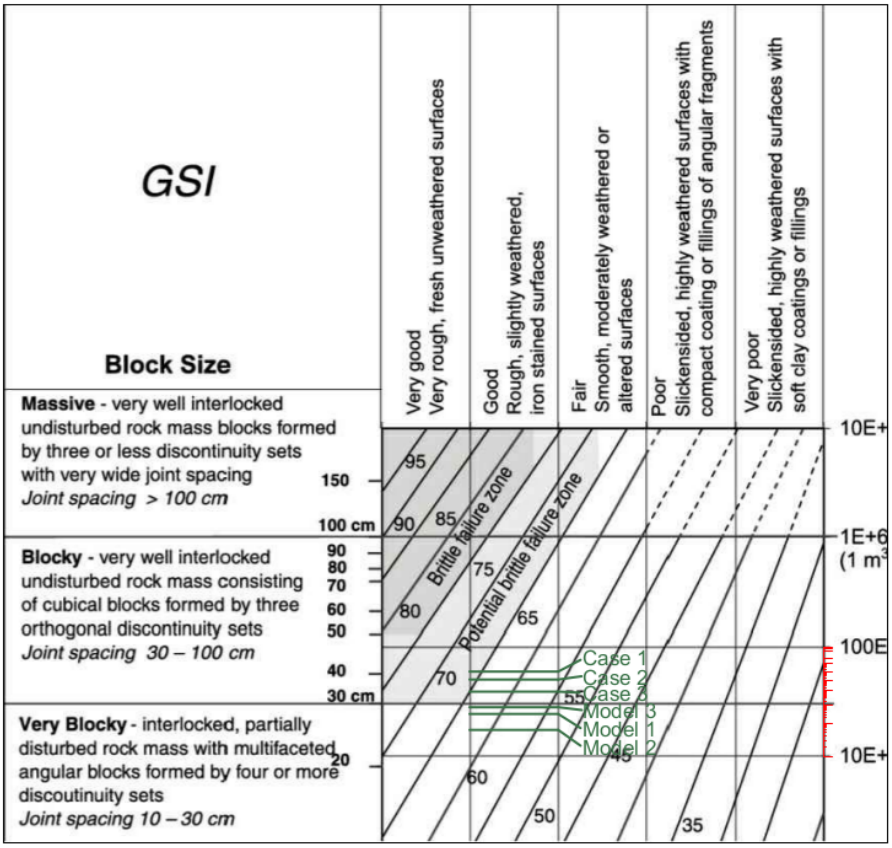

Figure 4.7: GSI for GT 2 with different models and different analytic calculations.

5 Conclusion

To determine an *in situ* block size distribution based on geophysical borehole measurements, different numerical models of a certain subsurface area were created. The aim was to evaluate different approaches to determine the block size distribution with different levels of simplification of the input data. In order to validate the methodology, a statistical DFN model with non–persistent discontinuities was compared to the results of surface block size measurements. For a second group of models, the persistence was neglected being the input parameter most difficult to determine and hence featuring the highest level of uncertainty.

The first model represents a deterministic DFN and served as a reference model for further investigations and therefore features the lowest level of simplification. The second one represents a DFN model based on statistical parameters with five joint sets. For the third model, these five joint sets were restricted to three and a diversification of the set orientations was implemented. The results of the third model were furthermore compared to block size calculations with an analytic formula.

First of all, a high correlation between the distributions from surface block size measurements and the DFN model with non–persistent joints is shown and thus the chosen modeling approach can be considered as an appropriate method for this investigations.

When comparing the different persistent models, it came out that some simplifications are permitted and others are facing difficulties. To be specific, the restriction from five to three joint sets is problematic, because this will yield a significant change in the block size distribution. In general, one can conclude that the mapping from a deterministic model to a statistical one, it is possible to obtain block size distributions that are similar in shape. If the entity of interest is not a reliable block size distribution for scientific purposes but the mean block size volume, all models can produce satisfying results. However, for any restriction to a lower number of joint sets (third model approach), certain subtleties must be implied. Here, it is crucial to reflect the geological inhomogeneities when choosing the artificial set clustering, which might be error-prone in situations with very discrete and diversely separated groups of

joints.

In practice, one can also utilize an analytic formula to determine the mean block volume, for a three–set configuration. It is advisable not to calculate one single value for the block volume using the mean value of the joint spacings, but rather compute a number of block volumes utilizing the original distributions of spacings. As shown in the course of this work, this can be done with Monte Carlo Simulations with little computational effort and was successfully compared to the computation with the original distributions of spacings.

Future investigations could compare our results of non–persistent modeling with different DFN models, such as Monte Carlo based simulations that use more realistic geometry features as an input.

Bibliography

Austrian Society for Geomechanics (2010). Guideline for the geotechnical design of underground structures with conventional excavation.

Barton, N., Lien, R., & Lunde, J. (1974). Engineering classification of rock masses for the design of tunnel support. *Rock Mechanics*, *6*(4), 189–236.

Bieniawski, Z. (1973). Engineering classification of jointed rock masses. *Civil Engineer in South Africa*, *15*(12), 353–343.

Cai, M., Kaiser, P., Uno, H., Tasaka, Y., & Minami, M. (2004). Estimation of rock mass deformation modulus and strength of jointed hard rock masses using the GSI system. *International Journal of Rock Mechanics and Mining Sciences*, *41*(1), 3–19.

Einstein, H. H. & Baecher, G. B. (1983). Probabilistic and statistical methods in engineering geology. *Rock Mechanics and Rock Engineering*, *16*(1), 39–72.

Elmouttie, M. & Poropat, G. (2012). A method to estimate in situ block size distribution. *Rock Mechanics and Rock Engineering*, *45*(3), 401–407.

Hoek, E., Kaiser, P. K., & Bawden, W. F. (1995). Support of underground excavations in hard rock.

Itasca Consulting Group Inc. (2013). 3-dimensional distinct element code plot command reference. Website. Section 6.

Kim, B. H., Cai, M., Kaiser, P. K., & Yang, H. S. (2006). Estimation of block sizes for rock masses with non-persistent joints. *Rock Mechanics and Rock Engineering*, *40*(2), 169–192.

Lei, Q., Latham, J.-P., & Tsang, C.-F. (2017). The use of discrete fracture networks for modelling coupled geomechanical and hydrological behaviour of fractured rocks. *Computers and Geotechnics*, *85*, 151–176.

Paillet, F., Barton, C., Luthi, S., Rambow, F., & Zemanek, J. (1990). Borehole imaging and its application in well logging - an overview. *Borehole Imaging, Society of Professional Well Log Analysts Inc.*, 3–23.

Palmström, A. (1995). *RMi - a rock mass characterization system for rock engineering purposes*. PhD thesis, Oslo University.

Palmström, A. (2005). Measurements of and correlations between block size and rock quality designation RQD. *Tunnelling and Underground Space Technology*, 362–377.

Söllner, P. (2014). Determination of the in situ block size distribution as a parameter for the rock mass characterization based on measurements and statistical methods. Master thesis, Graz University of Technology, Austria.

Wang, L. G., Yamashita, S., Sugimoto, F., Pan, C., & Tan, G. (2003). A methodology for predicting the in situ size and shape distribution of rock blocks. *Rock Mechanics and Rock Engineering*, *36*(2), 121–142.

Williams, J. H. & Johnson, C. D. (2000). Borehole-wall imaging with acoustic and optical televiewers for fractured-bedrock aquifer investigations. *Minerals and Geotechnical Logging Society*, 43–53.

Williams, J. H. & Johnson, C. D. (2004). Acoustic and optical borehole-wall imaging for fractured-rock aquifer studies. *Journal of Applied Geophysics*, *55*(12), 151–159.

Appendix A

Table 5.1: Input data containing 150 joints.

Dip [°]	DD [°]	x–value [m]	y–value [m]	z–value [m]
51.24	70.62	10.12	21.67	-3.32
58.61	80.68	10.12	21.67	-4.38
64.62	83.71	10.12	21.67	-4.65
59.41	84.44	10.12	21.67	-5.80
83.55	331.09	10.12	21.67	-6.73
85.12	343.46	10.12	21.67	-7.53
11.01	138.59	10.12	21.67	-8.04
83.71	337.19	10.12	21.67	-8.06
25.45	118.48	10.12	21.67	-8.30
66.95	97.59	10.12	21.67	-10.42
63.10	63.67	10.12	21.67	-11.33
18.01	328.54	10.12	21.67	-11.55
75.05	296.32	10.12	21.67	-12.48
43.83	97.72	10.12	21.67	-12.86
11.86	298.02	10.12	21.67	-12.98
71.00	313.14	10.12	21.67	-13.11
65.16	107.37	10.12	21.67	-13.83
58.74	99.82	10.12	21.67	-13.90
51.03	242.41	10.12	21.67	-15.92
34.79	240.52	10.12	21.67	-16.18
67.69	319.18	10.12	21.67	-16.62
69.80	332.13	10.12	21.67	-16.94
14.91	254.55	10.12	21.67	-17.07

33.78	241.09	10.12	21.67	-17.41
40.56	105.90	10.12	21.67	-17.79
74.12	303.69	10.12	21.67	-18.26
58.09	69.13	10.12	21.67	-19.16
79.51	295.10	10.12	21.67	-21.07
50.52	78.99	10.12	21.67	-21.74
54.50	104.44	10.12	21.67	-22.65
62.86	356.88	10.12	21.67	-22.66
62.00	310.02	10.12	21.67	-25.37
44.39	50.07	10.12	21.67	-25.91
77.55	250.86	10.12	21.67	-26.49
22.37	172.81	10.12	21.67	-26.93
25.37	176.29	10.12	21.67	-27.71
70.93	90.41	10.12	21.67	-28.19
37.29	195.51	10.12	21.67	-28.33
58.90	79.08	10.12	21.67	-28.89
54.41	86.05	10.12	21.67	-29.29
58.23	82.20	10.12	21.67	-29.75
52.64	101.53	10.12	21.67	-30.40
43.07	64.06	10.12	21.67	-30.56
72.51	355.91	10.12	21.67	-31.64
62.63	90.90	10.12	21.67	-32.91
38.77	39.62	10.12	21.67	-33.14
33.75	52.24	10.12	21.67	-34.14
16.24	257.55	10.12	21.67	-34.35
57.64	81.07	10.12	21.67	-34.77
49.83	75.44	10.12	21.67	-35.37
55.93	85.47	10.12	21.67	-35.42
34.40	98.24	10.12	21.67	-35.86
54.86	92.36	10.12	21.67	-36.14
23.94	219.63	10.12	21.67	-36.37
21.08	127.43	10.12	21.67	-38.76
79.46	62.33	10.12	21.67	-41.08
66.88	350.99	10.12	21.67	-43.95

58.37	62.02	10.12	21.67	-44.42
28.78	175.94	10.12	21.67	-45.29
66.97	86.92	10.12	21.67	-45.86
60.40	94.32	10.12	21.67	-45.98
49.18	86.92	10.12	21.67	-46.12
31.27	47.62	10.12	21.67	-47.32
53.92	87.65	10.12	21.67	-47.67
21.52	20.36	10.12	21.67	-48.31
50.08	85.66	10.12	21.67	-48.82
71.47	298.55	10.12	21.67	-64.77
57.76	82.89	16.90	22.25	-6.34
60.59	96.34	16.96	22.39	-6.77
60.45	103.23	17.00	22.48	-7.04
52.85	85.47	17.09	22.70	-7.68
84.61	358.02	17.42	23.47	-9.99
65.72	286.00	19.58	28.55	-25.17
80.42	350.62	19.89	29.28	-27.34
72.48	236.32	20.19	30.00	-29.48
87.29	357.53	21.18	32.33	-36.45
84.51	346.30	22.41	35.22	-45.07
85.43	331.80	22.77	36.06	-47.58
85.53	346.41	24.40	39.90	-59.03
52.14	71.52	18.68	17.69	-7.52
76.80	330.27	18.80	17.57	-7.89
61.23	84.31	18.98	17.39	-8.39
61.66	65.07	19.24	17.13	-9.14
80.21	246.41	21.47	14.90	-15.63
85.55	153.63	21.90	14.47	-16.87
85.26	340.48	22.81	13.56	-19.49
79.61	257.16	22.90	13.47	-19.77
77.02	328.81	23.98	12.39	-22.90
84.60	309.45	24.04	12.33	-23.07
74.59	344.90	24.12	12.25	-23.31
88.44	259.11	24.51	11.86	-24.44

53.01	338.60	24.85	11.52	-25.42
72.02	303.35	25.42	10.95	-27.08
76.81	233.40	26.01	10.36	-28.78
38.24	319.58	26.97	9.40	-31.57
73.15	311.24	27.01	9.36	-31.69
80.08	272.91	27.63	8.74	-33.48
87.58	342.92	28.25	8.12	-35.27
78.94	221.49	28.29	8.08	-35.40
31.23	245.53	28.47	7.90	-35.92
79.84	291.74	28.67	7.70	-36.51
82.23	337.80	28.95	7.42	-37.30
83.62	256.29	29.02	7.35	-37.50
60.06	300.13	29.77	6.60	-39.70
39.63	330.10	30.48	5.89	-41.74
47.08	326.38	30.78	5.59	-42.62
82.42	321.81	31.74	4.63	-45.40
81.61	308.64	31.92	4.45	-45.93
61.25	22.75	32.63	3.74	-47.99
89.32	325.40	33.04	3.33	-49.17
82.22	329.46	33.09	3.28	-49.33
89.08	189.80	33.36	3.01	-50.09
86.67	325.61	35.82	0.55	-57.24
88.20	333.72	36.18	0.19	-58.27
73.47	248.36	36.67	-0.30	-59.68
88.31	325.25	37.07	-0.70	-60.86
76.76	307.96	39.85	-3.48	-68.92
79.85	301.23	39.90	-3.53	-69.05
82.50	255.18	39.96	-3.59	-69.22
43.74	85.63	18.88	25.19	-8.58
72.73	149.02	19.48	25.45	-10.37
33.00	133.67	19.74	20.48	-10.60
35.38	54.66	21.11	19.11	-14.59
10.24	68.74	20.88	19.34	-13.92
15.44	50.38	21.14	19.08	-14.66

84.56	336.71	20.10	25.71	-12.22
7.10	117.48	21.76	18.46	-16.45
14.84	350.11	21.16	19.06	-14.73
28.71	23.42	22.42	17.80	-18.37
25.66	19.31	22.37	17.85	-18.24
30.83	241.11	23.62	16.60	-21.87
13.04	245.80	25.83	14.39	-28.27
16.25	271.30	26.79	28.55	-32.21
52.59	77.15	19.49	25.45	-10.40
55.46	100.44	19.71	25.55	-11.07
52.01	87.39	19.76	25.57	-11.21
56.12	85.19	19.81	25.59	-11.36
56.34	52.56	20.28	25.79	-12.76
58.23	60.41	20.30	25.80	-12.84
58.85	80.60	20.36	25.82	-13.00
72.88	305.85	24.40	27.54	-25.07
68.88	297.17	24.42	27.54	-25.12
68.24	89.42	28.62	29.33	-37.68
57.40	59.41	20.10	20.12	-11.66
60.97	60.37	20.37	19.85	-12.43
74.77	248.22	20.50	19.72	-12.80
33.21	326.01	21.57	26.33	-16.61
23.31	338.32	23.31	27.07	-21.81
38.24	305.24	22.45	26.71	-19.26
16.34	90.33	28.88	11.34	-37.11

Listing 5.1: 3DEC code for creating joints for the deterministic model.

```
new

def sys
        md = 'C:\\'
end
@sys

set directory @md

set atol 0.0229

poly brick 0 40 0 40 -40 0

def create_array
        array aa(500)
        array bb(500,5)
        array temp(1)
end
@create_array

def read_data
        file = '3DEC_Model1.txt'
        status = open(file,0,1)
        command
                print @status
        endcommand
        status = read(aa,500)
        command
                print @status
        endcommand
        loop n (1,500)
                loop m (1,5)
```

```
                        bb(n,m) = parse(aa(n),m)
                endloop
        endloop
        status = close
end
@read_data

def create_joints
        loop n (2,151)
                dip_star = bb(n,1)
                dd_star  = bb(n,2)
                x_star   = bb(n,3)
                y_star   = bb(n,4)
                z_star   = bb(n,5)

                command
                        jset dd @dd_star dip @dip_star n 1 origin
                        @x_star @y_star @z_star
                endcommand
        endloop
end
@create_joints



delete range x 0 10
delete range x 30 40

delete range y 0 10
delete range y 30 40

delete range z -40 -30
delete range z -10 0
```

```
def write_bv
        file = 'output.txt'
        status = open(file,1,1)
        temp(1) = 'Number'+' '+'BlockIndex'+' '+'BlockID'+' '
        +'BlockVolume'
        status = write(temp,1)

        bi = block_head
        ii = 1

        loop while bi # 0
                bvi = b_vol(bi)
                bid = b_id(bi)
                temp(1) = string(ii)+' '+string(bi)+' '
                +string(bid)+' '+string(bvi)
                status = write(temp,1)
                bi = b_next(bi)
                ii = ii + 1
        endloop

        status = close
end
@write_bv

return
```

Table 5.2: Spacing data for five sets.

Set 1 [m]	Set 2 [m]	Set 3 [m]	Set 4 [m]	Set 5 [m]
0.54	0.18	0.11	0.64	0.26
0.79	1.03	0.07	0.16	3.23
0.89	0.48	1.24	0.69	1.42
0.83	0.82	0.80	2.78	2.92
1.26	1.26	1.25	0.55	0.26
0.40	11.52	1.71	0.92	0.89
4.23	0.02	0.05	0.58	0.34
1.82	0.01	0.26	0.04	9.47
	1.17	2.10	2.34	0.78
	1.35	1.27	0.82	0.62
	0.52	1.20	1.55	5.99
	0.89	0.35	0.55	2.01
	0.93	1.59	1.96	2.38
	1.82	1.25	1.37	6.49
	6.72	0.37	0.42	3.00
	0.04	0.47	0.24	2.64
		0.06	0.28	2.54
		1.66	0.39	10.34
		0.28	0.10	3.31
		1.13	1.41	0.73
		0.53	0.14	0.07
		0.02	0.60	1.71
		0.11	0.38	1.78
		0.99	0.36	0.13
		0.14	0.03	3.48
		0.36	0.26	3.53
			0.17	2.83
			2.97	3.29
			2.01	4.33
			0.87	1.18

					0.07	4.60		
					0.08	0.88		
					0.72			
					0.21			
					0.69			
					0.26			
					0.16			
					0.38			
					0.54			
					1.09			
					0.41			
					0.08			
					0.08			
					0.85			
					0.05			
					0.10			
					14.85			
					0.52			
					0.45			
					1.51			
					0.47			
					1.30			
					20.10			

Table 5.3: Spacing data for three sets.

1a [m]	1b [m]	1c [m]	2a [m]	2b [m]	2c [m]	3a [m]	3b [m]	3c [m]
0.27	0.15	0.72	0.07	0.05	0.59	0.19	0.22	0.85
0.18	0.51	0.18	0.05	0.17	0.15	0.13	0.75	0.22
1.19	0.20	0.78	0.30	0.06	0.64	0.84	0.29	0.92
0.32	5.21	1.53	0.08	1.73	1.25	0.22	7.70	1.79
0.17	0.70	0.18	0.04	0.23	0.15	0.12	1.03	0.21
0.04	0.36	1.45	0.01	0.12	1.19	0.03	0.53	1.69

1.20	3.45	0.62	0.31	1.15	0.51	0.85	5.11	0.73
0.11	1.16	1.04	0.03	0.39	0.86	0.08	1.71	1.22
0.45	5.12	0.66	0.12	1.70	0.54	0.32	7.56	0.77
0.96	1.56	0.05	0.24	0.52	0.04	0.68	0.58	0.06
0.54	1.62	2.65	0.14	0.54	2.18	0.38	2.40	3.11
0.93	2.38	0.93	0.24	0.79	0.77	0.66	3.51	1.09
2.14	1.20	1.76	0.55	0.40	1.44	1.52	1.78	2.06
4.21	1.47	0.62	1.07	0.49	0.51	2.98	2.18	0.73
7.12	2.20	2.22	1.81	0.73	1.82	5.04	3.25	2.60
0.13	0.29	0.70	0.03	0.10	0.57	0.09	0.43	0.81
0.63	2.70	0.86	0.16	0.90	0.70	0.45	3.99	1.01
1.50	1.10	0.48	0.38	0.37	0.39	1.06	1.63	0.56
0.91	0.30	0.27	0.23	0.10	0.22	0.64	0.44	0.32
0.87	0.90	0.31	0.22	0.30	0.26	0.62	1.33	0.37
1.11	12.72	0.44	0.28	4.23	0.36	0.79	18.81	0.52
0.02	5.47	0.11	0.00	1.82	0.09	0.01	8.09	0.13
0.02		1.60	0.00		1.31	0.01		1.88
0.74		0.16	0.19		0.13	0.53		0.18
3.11		0.68	0.79		0.56	2.20		0.80
2.95		0.43	0.75		0.35	2.09		0.50
0.86		0.41	0.22		0.34	0.61		0.48
3.91		0.03	1.00		0.03	2.77		0.04
2.34		0.30	0.60		0.25	1.65		0.35
0.73		0.19	0.19		0.16	0.52		0.22
0.90		1.79	0.23		1.47	0.63		2.09
1.17		1.58	0.30		1.30	0.82		1.85
0.06		2.28	0.01		1.87	0.04		2.67
0.08		0.98	0.02		0.81	0.06		1.15
0.72		0.08	0.18		0.07	0.51		0.10
0.57		0.10	0.14		0.08	0.40		0.11
1.54		0.82	0.39		0.67	1.09		0.96
0.04		0.24	0.01		0.20	0.03		0.28
1.22		0.44	0.31		0.36	0.87		0.51
0.42		0.35	0.11		0.29	0.30		0.41

0.27	0.29	0.07	0.24	0.19	0.35
0.82	0.19	0.21	0.15	0.58	0.22
0.70	0.44	0.18	0.36	0.49	0.51
0.30	0.62	0.08	0.50	0.21	0.72
0.95	1.24	0.24	1.01	0.67	1.45
0.18	0.46	0.05	0.38	0.13	0.54
1.11	0.10	0.28	0.08	0.78	0.11
0.05	0.10	0.01	0.08	0.04	0.11
0.26	0.96	0.07	0.79	0.18	1.13
2.44	0.05	0.62	0.04	1.73	0.06
0.35	0.11	0.09	0.09	0.25	0.13
0.89	16.83	0.23	13.80	0.63	19.71
2.76	0.59	0.70	0.48	1.95	0.69
0.05	0.51	0.01	0.42	0.03	0.60
	0.99		0.81		1.16
	0.72		0.59		0.85
	0.53		0.43		0.62
	1.02		0.83		1.19
	0.45		0.37		0.53
	0.05		0.04		0.06
	1.22		1.00		1.43
	1.22		1.00		1.43
	0.09		0.08		0.11
	12.78		10.48		14.97
	7.42		6.08		8.69